# *p22phox C242T SNP inhibits inflammatory oxidative damage to endothelial cells and vessels*

Article

Accepted Version

DOI: 10.1161/CIRCULATIONAHA.116.021993

# $p22^{phox}$ C242T SNP Inhibits Inflammatory Oxidative Damage to Endothelial Cells and Vessels

**Running title:** *Meijles, et al.; $p22^{phox}$ C242T SNP inhibits endothelial ROS production*

Daniel N. Meijles, PhD[1,2]; Lampson M. Fan, PhD[3]; Maziah M. Ghazaly, PhD[2], Brendan Howlin, PhD[2]; Martin Krönke, MD[4]; Gavin Brooks, PhD[1]; Jian-Mei Li, MD. PhD[1*]

[1]Institute for Cardiovascular and Metabolic Research, School of Biological Sciences, University of Reading, UK; [2]Faculty of Engineering and Physical Sciences, University of Surrey, UK; [3]Department of Cardiology, Royal Berkshire Hospital, UK; [4]Institute for Medical Microbiology, Immunology and Hygiene, University of Cologne, Germany

**Address for Correspondence:**

Professor Jian-Mei Li

Institute for Cardiovascular and Metabolic Research

School of Biological Sciences

Harborne Building

University of Reading

Whiteknights

Reading RG6 6AS, UK

Tel: +44 (0)1183784419

Fax: +44 (0) 118 9310180

Email: jian-mei.li@reading.ac.uk

**Journal Subject Terms:** Genetic, Association Studies; Cell Biology/Structural Biology; Oxidant Stress; Vascular Biology; Inflammation

DOI: 10.1161/CIRCULATIONAHA.116.021993


## Abstract

***Background*—**T NADPH oxidase, by generating reactive oxygen species, is involved in the pathophysiology of many cardiovascular diseases and represents a therapeutic target for the development of novel drugs. A single-nucleotide polymorphism (SNP) C242T of the $p22^{phox}$ subunit of NADPH oxidase has been reported to be negatively associated with coronary heart disease (CHD) and may predict disease prevalence. However, the underlying mechanisms remain unknown.

***Methods and Results*—**Using computer molecular modelling we discovered that C242T SNP causes significant structural changes in the extracellular loop of $p22^{phox}$ and reduces its interaction stability with Nox2 subunit. Gene transfection of human pulmonary microvascular endothelial cells showed that C242T $p22^{phox}$ reduced significantly Nox2 expression but had no significant effect on basal endothelial $O_2^{\cdot-}$ production or the expression of Nox1 and Nox4. When cells were stimulated with TNFα (or high glucose), C242T $p22^{phox}$ inhibited significantly TNFα-induced Nox2 maturation, $O_2^{\cdot-}$ production, MAPK and NFκB activation and inflammation (all $p<0.05$). These C242T effects were further confirmed using $p22^{phox}$ shRNA engineered HeLa cells and $Nox2^{-/-}$ coronary microvascular endothelial cells. Clinical significance was investigated using saphenous vein segments from non CHD subjects after phlebectomies. TT (C242T) allele was common (prevalence of ~22%) and compared to CC, veins bearing TT allele had significantly lower levels of Nox2 expression and $O_2^{\cdot-}$ generation in response to high glucose challenge.

***Conclusions*—**C242T SNP causes $p22^{phox}$ structural changes that inhibit endothelial Nox2 activation and oxidative response to TNFα or high glucose stimulation. C242T SNP may represent a natural protective mechanism against inflammatory cardiovascular diseases.


**Key words:** genetics; endothelial dysfunction; NAD(P)H oxidase; oxidative stress; vessel

DOI: 10.1161/CIRCULATIONAHA.116.021993

## Introduction

Single-nucleotide polymorphisms (SNP) are one base variations in DNA sequences that occur in at least 1% of the population[1]. Although most SNPs have little or no effect on human health, some can predispose individuals to disease or have a major impact on the physiological response to environmental challenges or to drugs[1, 2]. Vascular endothelial cells express constitutively a Nox2 (also called gp91$^{phox}$) containing NADPH oxidase, which by generating superoxide ($O_2^-$) plays an important role in oxidative stress-related endothelial dysfunction and cardiovascular diseases (CVD)[3-7]. The Nox2 catalytic subunit requires p22$^{phox}$ in a 1:1 ratio to form the cytochrome $b_{558}$ complex to produce $O_2^-$, and structural changes of p22$^{phox}$ may affect its interaction with Nox2. In the context of Nox2-derived oxidative stress and CVD, SNPs of the p22$^{phox}$ have attracted significant attention recently.

The p22$^{phox}$ is encoded by the CYBA gene located on the long arm of chromosome 16 at position 24. It spans 8.5 kb and is composed of six exons and five introns encoding an open reading frame of approximately 600 bp[8]. The p22$^{phox}$ has three structural domains: 1) a hydrophobic N-terminal domain consisting of three transmembrane helices; 2) a hydrophilic extracellular region; and 3) a cytosolic tail featuring a proline rich region (PRR)[9, 10]. So far, seven SNPs of the p22$^{phox}$ gene have been reported i.e. C242T, A640G; C549T; A930G; A675T; C852G and C536T[11], and only two of them (C242T and C549T) are translated into the protein. The C549T SNP changes an Ala$^{174}$ to Val$^{174}$ without any reported significant functional effect[11]. In contrast, the C242T SNP changes His$^{72}$ to Tyr$^{72}$ that is located in the extracellular loop of the putative Nox2 binding region[12] and has been reported in several studies to be negatively associated with CVD, such as hypertension, atherosclerosis, and myocardial infarction and to reduce oxidative burst in neutrophils[11,13-15]. However, others have found that the C242T variant

had no effect on cardiovascular disease progression[16] or even increased ROS production in CVD arteries[17,18]. Given the contradictory evidence, it is important to elucidate the molecular mechanism responsible for the effects of $p22^{phox}$ C242T SNP on inhibiting endothelial Nox2 activity and vascular oxidative stress in order to ascertain its effect on CVD.

In this study, we used computer structural modeling plus molecular and biochemical approaches to elucidate the mechanism of $p22^{phox}$ C242T SNP inhibition of endothelial Nox2 activation and oxidative stress in response to TNFα or high glucose stimulation. Results were further confirmed using engineered $p22^{phox}$ depleted ($p22^{phox\text{-}depl}$) HeLa cells, primary coronary microvascular endothelial cells (CMEC) isolated from $Nox2^{-/-}$ mice and saphenous vein segments of patients without history of coronary heart diseases (CHD) after phlebectomies. We report for the first time that C242T SNP is linked to the $p22^{phox}$ extracellular domain morphological change that interferes with Nox2 binding stability and inhibits endothelial oxidative stress and inflammatory response to TNFα or high glucose challenges.

## Materials and methods

The *in silico* $p22^{phox}$ model was generated as reported previously by incorporating data from online prediction servers with the molecular operating environment (MOE; Chemical Computing Group Inc., Canada) and subjected to energy minimization using the AMBER99 forcefield[9,10]. The docking of $p22^{phox}$ with Nox2 peptides was performed in the MOE[10]. HapMap analysis of the CYBA gene was performed using the International HapMap Project (HapMap phase II+III; dbSNP b126) and six common *CYBA* SNPs were chosen from the National Centre for Biotechnology Information (NCBI) SNP database (dbSNP). Haplotype association was calculated using the Haplo-view analysis program (version 4.2) in the northern and western

European population (CEU). Human pulmonary microvascular endothelial cells (HPMEC-ST1.6R) were a kind gift from Dr R. Unger (Johannes Gutenberg University, Germany)[19]. Mouse CMEC were isolated from the hearts of ~12 week old Nox2$^{-/-}$ and WT mice and cultured as described previously[20,21]. The shRNA p22$^{phox}$ (p22$^{phox\text{-}depl}$) and shRNA scrambled control HeLa cells were generated as described previously[22] in the laboratory of Professor Krönke (University of Cologne, Germany). Segments of human saphenous vein were collected from 36 patients (without history of CHD) undergoing phlebectomies at a specialist vein unit. Informed consents were obtained from the patients and the project was approved by the local NHS and the university ethical committees according to UK regulation. The IRB approval was obtained according to the guidelines noted in the Circulation Instruction to Authors. The C to T substitution at position 242 in the CYBA coding sequence was examined as described previously[23]. ROS production was measured using four independent methods as described previously[24]: 1) Lucigenin-chemiluminescence; 2) DHE fluorescence HPLC assay with or without superoxide dismutase–polyethylene glycol (PEG-SOD)[4,25]; 3) DHE flow cytometry; and 4) DCF fluorescence.

See the online-only Data Supplement for a full description of materials and methods.

**Statistics**

Data were presented as means ± SD in figures. For cell culture experiments, results were taken from at least 3 independent cell cultures and gene transfections for each condition. In the case of CMEC isolation, 6 mice/per group were used for each isolation and the data presented were the means ± SD from at least 3 separate CMEC isolations. Comparisons were made by ANOVA with Bonferroni *post hoc* correction or as indicated in the figure legend. Values of $P<0.05$ were considered statistically significant.

DOI: 10.1161/CIRCULATIONAHA.116.021993

## Results

### Structural changes in p22$^{phox}$ associated with C242T SNP

Computer modeling was used to investigate potential protein structural changes linked to p22$^{phox}$ C242T SNP[9]. Our consensus p22$^{phox}$ model showed that His$^{72}$ (WT p22$^{phox}$) is located within the extra-cellular region of the p22$^{phox}$ (Figure 1A), which has been identified to be essential for interaction with Nox2[12,26]. The histidine residue contains a polar hydrophilic imidazole in comparison to the aromatic and hydrophobic tyrosine residue. The substitution of His$^{72}$ to Tyr$^{72}$ alters the conformation of the extracellular region as shown by the backbone side-view (Figure 1A, left panels) and top-view (Figure 1A, right panels). Root mean squared deviation (RMSD) calculations of extracellular structures of WT and C242T p22$^{phox}$ following energy minimization revealed significant difference between two structures (Figure 1C).

We next performed protein/protein docking of p22$^{phox}$ with a known Nox2 peptide (222-HGAERIVR-229) that corresponds to the Nox2 extracellular region involved in binding to p22$^{phox}$ in a previous report[27]. We found that the Nox2 peptide interacted successfully with the WT p22$^{phox}$ extracellular domain and formed a hydrogen-bond between Arg$^{226}$ of the Nox2 and Asn$^{86}$ of the p22$^{phox}$ (Figure 1B, upper panels). However, this interaction was lost in the C242T model (Figure 1B, lower panels). Further docking experiments were performed using two Nox2 peptides (peptide 1: 154-NFARKRIKNPEGGLY-168; peptide 2: 222-HGAERIVRG-230), which are located in the Nox2 extracellular domain and have been reported previously to be recognized by a Nox2 antibody (7D5)[27] (Figure 2). We found several important hydrogen bonds (labeled by H) formed between the Nox2 peptides and the WT p22$^{phox}$ configuration, which further illustrated the importance of Nox2 Arg$^{226}$ in stabilizing the interaction with WT p22$^{phox}$. However, these links were disrupted by the C242T p22$^{phox}$ configuration. We also performed

HapMap analysis of the CEU (European) population, and found that the C242T SNP is only in strong correlation ($r^2 = 0.99$) with one SNP located within a non-coding region of intron 4 (rs12933505; Figure 1D). Moreover, the genotyped allele frequency of the CC (WT) and the CT and TT variants is 53% and 47%, respectively. This confirms the functional effect of C242T SNP is independent of other known $p22^{phox}$ SNPs at the protein level.

**Effect of C242T SNP on endothelial Nox2 activity**

The functional effect of $p22^{phox}$ C242T SNP on human endothelial Nox2 activity was firstly investigated by site-directed mutagenesis followed by gene transfection of human pulmonary microvascular endothelial cells (HPMECs) with or without acute TNFα (100 unit/ml; 30 min) stimulation. HPMECs displayed low levels of $O_2^{\cdot-}$ production at basal conditions (without TNFα stimulation) whereas TNFα increased significantly the levels of $O_2^{\cdot-}$ production in cells either transfected with an empty vector or with WT $p22^{phox}$, without significant differences between them (Figure 3A). However, compared to WT $p22^{phox}$, C242T $p22^{phox}$ had no significant effect on endothelial basal $O_2^{\cdot-}$ production, but did significantly inhibit TNFα-induced $O_2^{\cdot-}$ production (Figure 3A; right panel). The enzymatic sources of TNFα-induced $O_2^{\cdot-}$ production in vector or WT $p22^{phox}$ transfected cells was confirmed using human Nox2ds-tat peptide (a specific inhibitor of Nox2)[28] and different enzyme inhibitors (Figure 3B). TNFα-induced $O_2^{\cdot-}$ production was inhibited significantly by Nox2ds-tat but not by NoxA1ds peptide (a specific inhibitor of Nox1, see Supplemental Figure 1) and was completely abolished by an $O_2^{\cdot-}$ scavenger (Tiron; 10mmol/L) which confirmed the detection of $O_2^{\cdot-}$. It was significantly inhibited by apocynin (100μmol/L, a Nox2 inhibitor) and diphenyliodium (DPI 20μmol/L, a flavoprotein inhibitor), but not by L-Nitroarginine-methyl-ester (L-NAME 100μmol/L, an eNOS inhibitor), oxypurinol (100μmol/L, a xanthine oxidase inhibitor) or rotenone (50μmol/L, a mitochondrial electron

transport chain inhibitor) (Figure 3B). Compared to WT $p22^{phox}$ transfected cells, C242T $p22^{phox}$ had no significant effect on Nox4 activity ($H_2O_2$ production) as shown using HEK293 cells (no endogenous Nox4 expression) co-transfected with Nox4 plus $p22^{phox}$ (Supplemental Figure 2). These data further confirmed a crucial role of Nox2-containing NADPH oxidase in TNFα-induced endothelial $O_2^{\cdot -}$ production.

The inhibitory effect of $p22^{phox}$ C242T on TNFα-induced endothelial $O_2^{\cdot -}$ production was further confirmed by two independent methods: DHE high-performance liquid chromatography (HPLC) detection of 2-OH-$E^+$ (Figure 3C) and the tiron-inhibitable DCF-fluorescence microscopy using intact adherent endothelial cells (Figure 3D).

**Effects of C242T $p22^{phox}$ on endothelial Nox subunit expression and binding to $p22^{phox}$**

The effects of $p22^{phox}$ C242T SNP on the basal levels of NADPH oxidase subunit expression was examined by Western blot. Compared to vector-transfected cells, the levels of $p22^{phox}$ expression were significantly increased in cells transfected with WT or C242T $p22^{phox}$, which confirmed the success of gene transfection (Figure 4A). Nox1 expression was nearly undetectable. We found that C242T $p22^{phox}$ reduced significantly Nox2 expression without significant effect on Nox4 or Nox2 regulatory subunits i.e. $p47^{phox}$, $p67^{phox}$, $p40^{phox}$ and Rac1/2 and Nox4 as compared to cells transfected with vector or WT $p22^{phox}$ (Figure 4A).

Nox2 antibody 7D5 recognizes specifically an extracellular domain of human Nox2 and the levels of antibody 7D5 binding have been successfully used previously to indicate the levels of Nox2 maturation (cell surface membrane expression and stable cytochrome *b* formation) in cells[27,29,30]. Using flow cytometry, we found that TNFα increased significantly antibody 7D5 binding to endothelial cells, and C242T $p22^{phox}$ reduced significantly the antibody 7D5 binding at both basal and in response to TNFα stimulation as compared to cells transfected with vector or

WT $p22^{phox}$ (Figure 4B). We then examined the effects of C242T $p22^{phox}$ on $p22^{phox}$ binding to Nox1, Nox2 and Nox4 by immuno-pull-down assay using $p22^{phox}$ antibody coated beads (Figure 4C). Supplemental Figure 3 showed the molecular weights on full gel presentation, and the protein levels detected in the whole cell homogenates were shown in Supplemental Figure 4. The levels of Nox1 pulled-down by $p22^{phox}$ were barely detectable, and we could not see a significant effect of C242T $p22^{phox}$ on Nox1. Under basal condition (vehicle stimulated), there was no significant difference in the levels of Nox2 or Nox4 pulled-down by $p22^{phox}$ beads between cells transfected with vector or WT or C242T $p22^{phox}$ (Figure 4C). TNFα stimulation (24 h) increased significantly the levels of Nox2 and reduced the levels of Nox4 pulled-down by $p22^{phox}$ beads in vector or WT $p22^{phox}$ transfected cells. However, in cells transfected with C242T $p22^{phox}$, TNFα-induced Nox2 binding to $p22^{phox}$ was significantly reduced, while the levels of Nox4 binding to $p22^{phox}$ remained at vehicle levels as compared to vector or WT $p22^{phox}$ transfected cells. Taken together our results strongly suggested that $p22^{phox}$ C242T morphology inhibits specifically the interaction stability between Nox2 and $p22^{phox}$ and reduced TNFα-induced Nox2 activation in endothelial cells.

**Effects of C242T $p22^{phox}$ on TNFα-induced $p22^{phox}$/$p47^{phox}$ binding and redox signaling through MAPKs and NF-κB in endothelial cells**

$p22^{phox}$, through its intracellular C-terminal domain, anchors $p47^{phox}$ to Nox2 in the membrane to activate NADPH oxidase. In our computer model, C242T SNP was predicted not to affect $p47^{phox}$ membrane translocation and binding to $p22^{phox}$. To confirm this, we prepared endothelial cell membrane fraction and examined for the membrane expression of $p47^{phox}$ by immunoblot (Figure 5A). Compared to vehicle control cells, TNFα stimulation significantly increased the levels of $p47^{phox}$ membrane expression without significant difference between vector and WT or

C242T $p22^{phox}$ transfected cells. We then immuno-precipitated $p47^{phox}$ and examined the levels of $p22^{phox}$ pulled down by $p47^{phox}$ beads and the levels of $p47^{phox}$ phosphorylation (Figure 5B). Compared to vehicle control cells, TNFα stimulation increased the levels of $p22^{phox}$/$p47^{phox}$ complex formation and $p47^{phox}$ phosphorylation without significant difference between cells transfected with vector and WT or C242T $p22^{phox}$. Membrane ROS production was shown in the Supplemental Figure 5. Once again, our data confirmed that the C242T $p22^{phox}$ inhibition of TNFα-induced endothelial $O_2^{\cdot-}$ production is specific to the Nox2 catalytic subunit.

Next, we examined the effect of C242T $p22^{phox}$ on TNFα-induced redox activation of extracellular regulated kinase-1/2 (ERK1/2), $p38^{MAPK}$ and NFκB in endothelial cells (Figure 5C). Compared to vehicle treated cells, TNFα stimulation increased significantly the levels of ERK1/2, $p38^{MAPK}$ and $NF\kappa B^{Ser311}$ phosphorylation in WT $p22^{phox}$ transfected cells (Figure 5C), and these were accompanied by significant increases in endothelial apoptosis detected by annexin-V flow cytometry (Figure 5D). Interestingly, these TNFα effects were significantly inhibited in cells transfected with C242T $p22^{phox}$. The levels of JNK phosphorylation was very low with no significant changes being detected after TNFα stimulation (data not shown).

**$p22^{phox}$ C242T inhibition of TNFα-induced endothelial vascular cell adhesion molecule-1 (VCAM-1) expression and inflammation**

TNFα plays a key role in the pathogenesis of atherosclerosis and many other cardiovascular disorders. In order to explore the clinical significance of C242T $p22^{phox}$ in inhibiting inflammatory endothelial dysfunction, we examined TNFα (24 h)-induced endothelial expression of VCAM-1 and NFkB nuclear translocation by immunofluorescence (Figure 6A). Compared to vehicle treated cells, TNFα increased significantly the levels of NFκB (green) in the nuclei and VCAM-1 expression (red) mainly around the plasma membrane in cells transfected with vector

or WT $p22^{phox}$, but not with C242T $p22^{phox}$ (Figure 6A). The inhibitory effect of $p22^{phox}$ C242T on TNFα-induced endothelial VCAM-1 expression was further confirmed by flow cytometry (Figure 6B).

We examined also TNFα-induced monocyte adhesion to endothelial cells using FITC-labelled U937 cells, and found that 24 h of TNFα stimulation increased significantly the number of monocytes attached to the endothelial monolayer in vector or WT $p22^{phox}$ transfected HPMEC but not in C242T $p22^{phox}$ transfected cells (Figure 6C). The inhibitory effect of C242T $p22^{phox}$ on endothelial Nox2 activation was further confirmed using cells stimulated with high level of glucose (25 mmol/L) (Supplemental Figure 6).

**Experiments using engineered $p22^{phox\text{-}depl}$ HeLa cells**

In order to confirm that our results of C242T $p22^{phox}$ would not be affected by the intrinsic $p22^{phox}$ protein expressed in HPMECs, we used engineered HeLa cells after $p22^{phox}$ depletion using a specific short-hairpin RNA (shRNA). A scrambled shRNA was used as controls in all experiments. The absence of $p22^{phox}$ protein in $p22^{phox\text{-}depl}$ cells was confirmed by immunoblotting (Figure 7A) and immunofluorescence (Figure 7B and Supplemental Figure 7). The $p22^{phox}$ protein was detected in scrambled shRNA treated cells and in $p22^{phox\text{-}depl}$ cells after gene transfection of WT or C242T $p22^{phox}$ (Figure 7A and B). Compared to scrambled shRNA treated control cells, the levels of both Nox2 and Nox4 were low in $p22^{phox\text{-}depl}$ cells, and increased to control levels after $p22^{phox}$ gene transfection. However, compared to WT $p22^{phox}$ transfected cells, the levels of Nox2 (but not Nox4) remained significantly lower in C242T $p22^{phox}$ transfected cells (Figure 7A). The levels of Nox1 expression was unaffected by the absence of $p22^{phox}$. We then examined Nox2 maturation recognized by Nox2 antibody 7D5 and analyzed by flow cytometry (Figure 7C). Compared to scrambled shRNA control cells, $p22^{phox\text{-}}$

$^{depl}$ cells had significantly lower (19.5±2.8%) levels of Nox2 maturation, and this was restored to the control levels after WT $p22^{phox}$ transfection. However, the levels of Nox2 maturation remained significantly lower (58.7±2.3%) in C242T $p22^{phox}$ transfected cells.

The levels of $O_2^{\cdot-}$ production by these cells were examined by lucigenin chemiluminescence in cell homogenates (Figure 7D, left panel) and the tiron-inhibitable DHE fluorescence flow cytometry (Figure 7D, right panel). Compared to scrambled shRNA treated control cells, $p22^{phox\text{-}depl}$ cells had significantly lower levels of $O_2^{\cdot-}$ production under basal condition and lost completely the $O_2^{\cdot-}$ response to TNFα stimulation. TNFα-induced $O_2^{\cdot-}$ production was restored to the scrambled shRNA control levels after gene transfection of WT $p22^{phox}$. However, gene transfection of C242T $p22^{phox}$ only restored the basal but not the TNFα-induced $O_2^{\cdot-}$ production (Figure 7D). Reduced interaction between C242T $p22^{phox}$ and Nox2 (but not Nox4) after TNFα stimulation was further confirmed in $p22^{phox\text{-}depl}$ cells (Supplemental Figure 8).

**Experiments using $Nox2^{-/-}$ coronary microvascular endothelial cells (CMEC)**

In order to further confirm if C242T $p22^{phox}$ affected only Nox2 (but not Nox4 and/or Nox1), we isolated primary CMEC from wild-type and Nox2 knockout mice. Cells were then subjected to gene transfection and examined for $O_2^{\cdot-}$ production with or without TNFα stimulation (Supplemental Figure 9). Under basal conditions, $Nox2^{-/-}$ cells produced less $O_2^{\cdot-}$ compared to WT cells without significant differences between cells transfected with vector or WT $p22^{phox}$ or C242T $p22^{phox}$. TNFα stimulation greatly increased the levels of $O_2^{\cdot-}$ production in WT CMEC transfected with vector or WT $p22^{phox}$. Compared to WT $p22^{phox}$ transfected cells, $p22^{phox}$ C242T inhibited significantly the levels of TNFα-induced $O_2^{\cdot-}$ production (40±14% reduction) (Supplemental Figure 9). In contrast, TNFα increased only slightly (but still statistically

significant) the levels of $O_2^{\cdot-}$ production by Nox2$^{-/-}$ CMEC and there was no significant difference between cells transfected with vector, WT or C242T p22$^{phox}$. It was clear that C242T p22$^{phox}$ had no significant effect on TNFα-induced endothelial $O_2^{\cdot-}$ production in the absence of Nox2.

**C242T SNP frequency and inhibition of Nox2 expression and high-glucose induced ROS production in human saphenous veins**

In order to investigate the clinical significance, we genotyped 36 saphenous vein samples collected from patients after phlebectomies who had no history of coronary heart disease. We found that 50% samples were wild-type (CC), ~27.8% were heterozygotes (CT) and ~22.2% had p22$^{phox}$ C242T SNP (TT) with ~36.1% frequency of T allele appearance (Figure 8A). Dot-blot showed a significant reduction of Nox2 expression in TT vessels in comparison to CC vessels (Figure 8B). Immunofluorescence images revealed that the reduction of Nox2 was mainly in the endothelium (Figure 8D). It is well known that superoxide ($O_2^{\cdot-}$) reacts with nitric oxide (NO) to form peroxynitrite which modifies tyrosine residue to form 3-nitrotyrosine (3NT), a biomarker of tissue oxidative damage. We found significantly lower levels of 3-nitrotyrosine (3NT) detected in TT samples as compared to CC samples (Figure 8C). When the vessels were challenged *ex vivo* with high level of glucose (25 mmol/L) for 24 h, TT samples had significantly less ROS production in comparison to CC sample (Figure 8E). Superoxidase dismutase was used to confirm the detection of $O_2^{\cdot-}$.

**Discussion**

The NADPH oxidase, by generating $O_2^{\cdot-}$, plays a crucial role in the inflammatory response involved in the pathogenesis of many cardiovascular diseases. The p22$^{phox}$ is an integral

membrane-associated subunit of NADPH oxidase responsible for assembling and stabilising Nox subunits into an active enzyme complex for ROS production[8]. A number of clinical studies have reported that individuals bearing a naturally-occurring $p22^{phox}$ C242T SNP have diminished $O_2^{\cdot-}$ production and are less susceptible to inflammatory cardiovascular diseases[11,23,31,32]. However, little progress has been made to clarify the underlying molecular mechanisms. For the first time, our study provides scientific evidence that $p22^{phox}$ C242T SNP causes $p22^{phox}$ structural changes in the extracellular domain that are unfavorable for Nox2 maturation and activation, and inhibits endothelial $O_2^{\cdot-}$ production in response to TNFα or high glucose stimulation.

A number of findings have been made by the current study in understanding the mechanism of $p22^{phox}$ C242T SNP inhibition of Nox2 activation: 1) There is a significant structural difference between WT and the C242T $p22^{phox}$ protein extracellular region that is important for Nox2 maturation[12,33]; 2) C242T $p22^{phox}$ structure compromises its binding stability with Nox2. The complex formed between Nox2 and C242T $p22^{phox}$ is less stable due to the lacking of crucial hydrogen bonds to bind them together. Unstable binding may led to Nox2 protein degradation and this may explain the low levels of Nox2 detected in C242T $p22^{phox}$ transfected cells and in vein samples of TT individuals.

The C242T SNP does not affect Nox1 because the $Arg^{226}$ (crucial for the hydrogen bond formation to stabilize the interaction between Nox2 and WT $p22^{phox}$) is replaced by Gly in Nox1. Furthermore, the putative epitope 1 (160-IKNP-163) that is required to interact with $p22^{phox27}$ is absent in Nox1 (Supplemental Table 1). Nevertheless, Nox1 expression is extremely low in endothelial cells and is not a major source of endothelial ROS production in inflammation. Nox4 is highly expressed in endothelial cells. Nox4 generates $H_2O_2$ and has been found to be involved mainly in cellular growth and normal function, and is protective to cardiovascular function[34,35].

Using immunoblotting, real-time PCR (Supplemental Figure 10) and co-immunoprecipitation we have shown that C242T $p22^{phox}$ does not inhibit Nox4 expression or its complex formation with $p22^{phox}$. Furthermore, using HEK293 cells that do not express endogenous Nox4, we have demonstrated that (after Nox4 gene transfection) C242T $p22^{phox}$ has no effect on Nox4 activity (Supplemental Figure 2). Under the basal condition (without TNFα), C242T $p22^{phox}$ has no effect on endothelial Nox2 mRNA expression (Supplemental Figure 10) but reduces the protein levels of Nox2 expression and Nox2 maturation. These results strongly suggest that the effect of C242T $p22^{phox}$ on Nox2 expression is post-translational. When the cells were challenged by TNFα, the inhibitory effect of C242T $p22^{phox}$ on TNFα-induced Nox2 mRNA expression (Supplemental Figure 10) is more likely due to reduced levels of oxidative stress and redox signaling (such as NFκB) that impair Nox2 transcription in C242T $p22^{phox}$ transfected cells.

Nox2 has low basal activity in endothelial cells and generates a small quantity of $O_2^{\cdot-}$ mainly used for redox-signaling under physiological conditions. Another important finding by the current study is that C242T $p22^{phox}$ configuration can still allow Nox2 to bind and support a low basal level of $O_2^{\cdot-}$ production. However, when the cells face challenge by TNFα C242T $p22^{phox}$ could not support a full Nox2 activation and thereby inhibits endothelial oxidative response to TNFα and protects endothelial cells from inflammation and cell apoptosis. The inhibitory effect of C242T $p22^{phox}$ on TNFα-induced endothelial ROS production by Nox2 was examined using four independent complementary methods: lucigenin-chemiluminecscence; DHE-HPLC; DHE-flow cytometry and DCF fluorescence microscopy and further confirmed by experiments using Nox2ds-tat, several enzyme inhibitors and $Nox2^{-/-}$ CMEC.

Previously, C242T SNP was reported to form a haplotype correlated with two other $p22^{phox}$ SNPs: namely the C521T (rs1049254) and A24G (rs1049255) that reduced Nox2-activity

in Epstein-Barr virus-transformed B-lymphocytes isolated from 50 healthy individuals of an Utah pedigree[33]. However, our HapMap analysis could not identify a close correlation of C242T with any other SNPs of $p22^{phox}$ currently identified within the HapMap database. Our results strongly suggest that the functional effects of C242T SNP on NADPH oxidase are independent of any other known protein-translated $p22^{phox}$ SNPs.

Using engineered $p22^{phox\text{-}depl}$ HeLa cells we further demonstrated that in the absence of $p22^{phox}$, both Nox2 and Nox4 expressions were reduced, and could be restored after gene transfection of WT $p22^{phox}$. However, gene transfection of C242T $p22^{phox}$ into $p22^{phox\text{-}depl}$ cells only fully restored the expression of Nox4 (but not Nox2). When cells were subjected to TNFα challenge, C242T $p22^{phox}$ transfected cells failed to increase $O_2^{\cdot-}$ production. C242T $p22^{phox}$ had no significant effect on its interaction with $p47^{phox}$ or on TNFα-induced $p47^{phox}$ phosphorylation. However, due to the inhibitory effect of C242T $p22^{phox}$ on Nox2 activation, TNFα-induced ROS production and redox-signaling through MAPK and NFκB were compromised in endothelial cells, which protected endothelial cells from oxidative damage and inflammation.

Increased VCAM-1 expression and monocyte adherence to endothelial cells are crucial steps in the pathogenesis of inflammatory cardiovascular diseases. The clinical significance of C242T $p22^{phox}$ was demonstrated by showing that TNFα-induced endothelial VCAM-1 expression and monocyte adherence to endothelial cells were significantly inhibited in C242T $p22^{phox}$ transfected cells. Saphenous veins are commonly used as conduits for bypass surgery to treat coronary artery diseases. Information on the $p22^{phox}$ genetic variation can predict graft oxidative response to environment challenge and help clinical management of vein grafts. We found a genetic frequency of 22.2% for TT genotype (36.1% for T allele) in our samples, which is in accordance to those reported previously for control samples or for the general population[36-

[38]. Using both dot-blotting and immunofluorescence, we confirmed that $p22^{phox}$ C242T SNP is indeed associated with reduced Nox2 expression mainly in the endothelium, and TT vessels had significantly less ROS generation in response to high glucose challenge as compared to CC vessels.

Limitations need to be considered in the interpretation of our $p22^{phox}$ molecular models. Although our computer models are supported by extensive cell and molecular experimental data, the structural models still need to be confirmed by X-ray crystallography or nuclear magnetic resonance spectroscopy.

In summary, this is the first report to describe the mechanism of $p22^{phox}$ C242T SNP in inhibiting Nox2 activity and protecting endothelial cells from TNFα-induced oxidative damage and inflammation. $p22^{phox}$ C242T SNP represents a natural protective mechanism against inflammatory cardiovascular diseases. The molecular mechanism reported here can be further explored for novel drug development.

**Funding Sources:** This work was funded by the British Heart Foundation (PG/14/85/31161) and the Wellcome Trust (Project Grant 07863/Z/05/Z).

**Conflict of Interest Disclosures:** None.

**References:**

1. Shastry BS. SNP alleles in human disease and evolution. *J Hum Genet.* 2002;47:561-566.

2. Thanassoulis G, Vasan RS. Genetic cardiovascular risk prediction. Will we get there? *Circulation.* 2010;122:2323-2334.

3. Lassègue B, Martin AS, Griendling KK. Biochemistry, physiology, and pathophysiology of NADPH oxidase in the cardiovascular system. *Circ Res.* 2012;110:1364-1390.

4. Fan LM, Douglas G, Bendall JK, McNeill E, Crabtree MJ, Hale AB, Mai A, Li JM, McAteer

MA, Schneider JE, Choudhury RP, Channon KM. Endothelial Cell-Specific ROS Production Increases Susceptibility to Aortic Dissection. *Circulation.* 2014;129:2661-2672.

5. Du J, Fan LM, Mai A, Li J-M. Crucial roles of Nox2-derived oxidative stress in deteriorating the function of insulin receptor and endothelium in dietary obesity of middle-aged mice. *Br J Pharmacol.* 2013;170:1064-1077.

6. Li J-M, Fan LM, George VT, Brooks G. Nox2 regulates endothelial cell cycle arrest and apoptosis via $p21^{cip1}$ and p53. *Free Radic Biol Med.* 2007;43:976-986.

7. Li J-M, Shah AM. Endothelial cell superoxide generation: Regulation and relevance for cardiovascular pathophysiology. *Am J Physiol Regul Integr Comp Physiol.* 2004;287:R1014-1030.

8. Dinauer MC, Pierce EA, Bruns GA, Curnutte JT, Orkin SH. Human neutrophil cytochrome b light chain (p22-*phox*). Gene structure, chromosome location, and mutations in cytochrome-negative autosomal recessive chronic granulomatous disease. *J Clin Invest.* 1990;86:1729-1737.

9. Meijles D, Howlin BJ, Li J-M. Consensus in silico computational modelling of the $p22^{phox}$ subunit of the NADPH oxidase. *Comput Biol Chem.* 2012;39:6-13.

10. Meijles DN, Fan LM, Howlin BJ, Li JM. Molecular insights of p47phox phosphorylation dynamics in the regulation of NADPH oxidase activation and superoxide production. *J Biol Chem.* 2014;289:22759-22770.

11. San José G, Fortuño A, Beloqui O, Diez J, Zalba G. NADPH oxidase CYBA polymorphisms, oxidative stress and cardiovascular diseases. *Clin Sci.* 2008;114:173-182.

12. Zhu Y, Marchal CC, Casbon AJ, Stull N, von LK, Knaus UG, Jesaitis AJ, McCormick S, Nauseef WM, Dinauer MC. Deletion mutagenesis of p22phox subunit of flavocytochrome b558: identification of regions critical for gp91phox maturation and NADPH oxidase activity. *J Biol Chem.* 2006;281:30336-30346.

13. Soccio M, Toniato E, Evangelista V, Carluccio M, De Caterina R. Oxidatrive stress and cardiovascular risk: the role of vascular NAD(P)H oxidase and its genetic variants. *Eur J Clin Invest.* 2005;35:305-314.

14. Jones LC, Hingorani AD. Genetic regulation of endothelial function. *Heart.* 2005;91:1275-1277.

15. Wythe KE, Wang S, Griendling KK, Dikalov SI, Austin H, Rao S, Fink B, Harrison DG, Zafari AM. C242T CYBA polymorphism of the NADPH oxidase is associated with reduced respiratory burst in human neutrophils. *Hypertension.* 2004;43:1246-1251.

16. Zafari AM, Davidoff MN, Austin H, Valppu L, Cotsonis G, Lassegue B, Griendling KK. The A640G and C242T p22(phox) polymorphisms in patients with coronary artery disease. *Antioxid*

*Redox Signal.* 2002;4:675-680.

17. Cahilly C, Ballantyne CM, Lim D-S, Gotto A, Marian AJ. A variant of p22, involved in generation of reactive oxygen species in the vessel wall, is associated with progression of coronary atherosclerosis. *Circ Res.* 2000;86:391-395.

18. Nasti S, Spallarossa P, Altieri P, Garibaldi S, Fabbi P, Polito L, Bacino L, Brunelli C, Barsotti A, Ghigliotti G. C242T polymorphism in CYBA gene (p22phox) and risk of coronary artery disease in a population of Caucasian Italians. *Dis Markers.* 2006;22:167-173.

19. Unger RE, Krump-Konvalinkova V, Peters K, Kirkpatrick CJ. In vitro expression of the endothelial phenotype: Comparative study of primary isolated cells and cell lines, including the novel cell line HPMEC-ST1.6R. *Microvascular Res.* 2002;64:384-397.

20. Li J-M, Mullen AM, Shah AM. Phenotypic properties and characteristics of superoxide production by mouse coronary microvascular endothelial cells. *J Mol Cell Cardiol.* 2001;33:1119-1131.

21. Fan LM, Teng L, Li J-M. Knockout of $p47^{phox}$ uncovers a critical role of $p40^{phox}$ in reactive oxygen species production in microvascular endothelial cells. *Arterioscler Thromb Vasc Biol.* 2009;29:1651-1656.

22. Yazdanpanah B, Wiegmann K, Tchikov V, Krut O, Pongratz C, Schramm M, Kleinridders A, Wunderlich T, Kashkar H, Utermohlen O, Bruning JC, Schutze S, Kronke M. Roboflavin kinase couples TNF receptor 1 to NADPH oxidase. *Nature.* 2009;460:1159-1163.

23. Guzik TJ, West NEJ, Black E, McDonald D, Ratnatunga C, Pillai R, Channon KM. Functional effect of the C242T polymorphism in the NAD(P)H oxidase p22phox gene on vascular superoxide production in atherosclerosis. *Circulation.* 2000;102:1744-1747.

24. Fan LM, Li JM. Evaluation of methods of detecting cell reactive oxygen species production for drug screening and cell cycle studies. *J Pharmacol Toxicol Methods.* 2014;70:40-47.

25. Teng L, Fan LM, Meijles D, Li J-M. Divergent effects of $p47^{phox}$ phosphorylation at S303-4 or S379 on tumor necrosis factor-α signaling via TRAF4 and MAPK in endothelial cells. *Arterioscler Thromb Vasc Biol.* 2012;32:1488-1496.

26. Campion Y, Jesaitis AJ, Nguyen MVC, Grichine A, Herenger Y, Baillet A, Berthier S, Morel F, Paclet M-H. New p22-phox monoclonal antobodies: Identification of a conformational probe for cytochromeb558. *J Innate Immun.* 2009;1:556-569.

27. Burritt JB, Deleo FR, McDonald CL, Prigge JR, Dinauer MC, Nakamura M, Nauseef WM, Jesaitis AJ. Phage display epitope mapping of human neutrophil flavocytochrome b558. Identification of two juxtaposed extracellular domains. *J Biol Chem.* 2001;276:2053-2061.

28. Csanyi G, Cifuentes-Pagano E, Al G, I, Ranayhossaini DJ, Egana L, Lopes LR, Jackson HM,

Kelley EE, Pagano PJ. Nox2 B-loop peptide, Nox2ds, specifically inhibits the NADPH oxidase Nox2. *Free Radic Biol Med.* 2011;51:1116-1125.

29. Yamauchi A, Yu L, Potgens AJ, Kuribayashi F, Nunoi H, Kanegasaki S, Roos D, Malech HL, Dinauer MC, Nakamura M. Location of the epitope for 7D5, a monoclonal antibody raised against human flavocytochrome b558, to the extracellular peptide portion of primate gp91phox. *Microbiol Immunol.* 2001;45:249-257.

30. Taylor RM, Dratz EA, Jesaitis AJ. Invariant local conformation in p22phox p.Y72H polymorphisms suggested by mass spectral analysis of crosslinked human neutrophil flavocytochrome b. *Biochimie.* 2011;93:1502-1509.

31. Inoue N, Kawashima S, Yamada K, Akita H, Yokoyama M. Polymorphism of the NADH/NADPH oxidase p22 phox gene in patients with coronary artery disease. *Circulation.* 1998;97:135-137.

32. Schächinger V, Britten MB, Dimmeler S, Zeiher AM. NADH/NADPH oxidase p22 phox gene polymorphism is associated with improved coronary endothelial vascular function. *Eur Heart J.* 2001;22:96-101.

33. Bedard K, Attar H, Bonnefont J, Jaquet V, Borel C, Plastre O, Stasia M-J, Antonarakis SE, Krause K-H. Three common polymorphisms in the CYBA gene from a haplotype associated with decreased ROS generation. *Hum Mutat.* 2009;30:1123-1133.

34. Li Y, Mouche S, Sajic T, Veyrat-Durebex C, Supale R, Pierroz D, Ferrari S, Negro F, Hasler U, Feraille E, Moll S, Meda P, Deffert C, Montet X, Krause K-H, Szanto I. Deficiency in the NADPH oxidase 4 predisposes towards diet-induced obesity. *International J Obesity.* 2012;36:1503-1513.

35. Clempus RE, Sorescu D, Dikalova AE, Pounkova L, Jo P, Sorescu GP, Schmidt HH, Lassegue B, Griendling KK. Nox4 is reguired for maintenance of the differentiated vascular smooth muscle cell phenotype. *Arterioscler Thromb Vasc Biol.* 2007;27:42-8.

36. de Oliveira Alvim R, Santos PC, Dias RG, Rodrigues MV, de Sa Cunha R, Mill JG, Junior WN, Krieger JE, Pereira AC. Association between the C242T polymorphism in the p22phox gene with arterial stiffness in the Brazilian population. *Physiol Genomics.* 2012;44:587-592.

37. Najafi M, Alipoor B, Shabani M, Amirfarhangi A, Ghasemi H. Association between rs4673 (C/T) and rs13306294 (A/G) haplotypes of NAD(P)H oxidase p22phox gene and severity of stenosis in coronary arteries. *Gene.* 2012;499:213-217.

38. Xu Q, Yuan F, Shen X, Wen H, Li W, Cheng B, Wu J. Polymorphisms of C242T and A640G in CYBA gene and the risk of coronary artery disease: a meta-analysis. *PLoS One.* 2014;9:e84251.

DOI: 10.1161/CIRCULATIONAHA.116.021993

## Clinical Perspective

NADPH oxidase, by generating reactive oxygen species, is involved in the pathophysiology of many cardiovascular diseases and represents a therapeutic target for the development of novel drugs. A number of clinic studies have reported that individuals bearing a naturally-occurring $p22^{phox}$ C242T single-nucleotide polymorphism (SNP) have diminished ROS production in the cardiovascular system and are less susceptible to inflammatory cardiovascular diseases. However, little progress has been made to clarify the underlying molecular mechanisms. The current study using computer molecular modelling plus cell and molecular techniques provides scientific evidence that $p22^{phox}$ C242T SNP causes $p22^{phox}$ structural changes in the extracellular domain that compromises its binding stability with Nox2 (the catalytic subunit of the NADPH oxidase) and reduces the levels of Nox2 protein expression and maturation. In response to TNFα challenge, C242T $p22^{phox}$ inhibits endothelial NADPH oxidase $O_2^{\cdot-}$ production, inflammatory VCAM-1 expression and monocyte adherence to endothelial cells. Clinical significance was investigated using saphenous vein segments from non-coronary heart disease subjects after phlebectomies. TT (C242T) allele was common (prevalence of ~22%) and compared to CC, veins bearing TT allele had significantly lower levels of Nox2 expression and $O_2^{\cdot-}$ generation in response to high glucose challenge. C242T SNP may represent a natural protective mechanism against inflammatory cardiovascular diseases. The molecular mechanism reported in this study can be further explored for novel drug development.

DOI: 10.1161/CIRCULATIONAHA.116.021993

**Figure Legends:**

**Figure 1.** Computer modelling of $p22^{phox}$ structural changes associated with C242T SNP. (A) Morphological differences between WT and C242T $p22^{phox}$ structures (ribbon presentation). (B) Docking of a Nox2-peptide (222-HGAERIVR-229) (skeleton in left panels and silver-space-fill in right panels) with $p22^{phox}$ extracellular domain (ribbon). Nox2 peptide interacts and forms an H-bond with the $N^{86}$ (ball and stick presentation) of WT $p22^{phox}$ but not with the $N^{86}$ of C242T $p22^{phox}$. (C) RMSD calculations of the extracellular domain structural differences between WT and C242T $p22^{phox}$ following energy minimization. n=3 independent investigators. *$p<0.05$ for C242T values versus WT values (Mann-Whitney U-test). (D) Linkage disequilibrium (LD) plot from Haplo-view of common genotyped SNPs within the *CYBA* ($p22^{phox}$) gene. The darker a diamond appears, the greater the correlation ($r^2$ x 100) between the respective genotyped *CYBA* polymorphisms. The C242T SNP (rs4673) is outlined.

**Figure 2.** Docking of two Nox2 peptides with $p22^{phox}$ extracellular domain. Images are shown as a tiled 45 degrees side-view/top-view. Two Nox2 peptides (peptide 1: 154-NFARKRIKNPEGGLY-168; peptide 2: 222-HGAERIVRG-230) used for the docking have been reported previously to be the extracellular epitopes of Nox2 recognised by an antibody (7D5) to Nox2. WT $p22^{phox}$ configuration forms several hydrogen bonds (short grey dashed lines labelled by H) with Nox2 peptides. The location of Nox2 $Arg^{226}$ is indicated. However, these interactions were lost in the C242T $p22^{phox}$ configuration. Red ribbons represent alpha helix.

**Figure 3.** The effect of $p22^{phox}$ C242T SNP on HPMEC ROS production. (A) Kinetic measurement of $O_2^{\cdot-}$ production. Area under curve (AUC) was calculated for each sample.

*$p$<0.05 for TNFα AUC values verses vehicle AUC values analyzed by unpaired t-test with Welch's correction. (B) Inhibition of $O_2^{\cdot-}$ production measured by lucigenin-chemiluminescence. Left panel: Nox2ds-tat peptide; Right panel: Effects of different enzyme inhibitors presented as percentages to TNFα values without inhibitor (filled bar). *$p$<0.05 for indicated values versus vehicle values under the same gene transfection. †$p$<0.05 for indicated values verses TNFα values (filled bar) under the same gene transfection. (C) $O_2^{\cdot-}$ production (2-OH-E) measured by DHE-HPLC. The amount of 2-OH-E was quantified against a standard curve and expressed as nmol/mg protein. (D) Intracellular ROS production examined by DCF fluorescence microscopy. Tiron was used to confirm the detection of $O_2^{\cdot-}$. (C-D) *$p$<0.05 for TNFα values verses vehicle values under the same gene transfection. †$p$<0.05 for indicated values versus WTp22 TNFα values. Sample size (A-C): n=4 independent experiments; (D): n=3 independent experiments.

**Figure 4.** NADPH oxidase subunit expression, Nox2 maturation and binding to $p22^{phox}$ in HPMEC. (A) Western blots. Optical densities (OD) of protein bands of $p22^{phox}$, Nox1, Nox2, Nox4, $p47^{phox}$, $p67^{phox}$, $p40^{phox}$ and Rac1/2 were quantified and normalized to the levels of α-tubulin (loading control) detected in the same samples. (B) Flow cytometry for the binding of Nox2 antibody (7D5). *$p$<0.05 for indicated values versus to vector values. †$p$<0.05 for indicated values versus WT values. (C) Left panel: $p22^{phox}$ was immunoprecipited (IP) followed by immunoblotting (IB) of Nox1, Nox2 and Nox4. Right panels: Optical densities (OD) of protein bands were quantified and normalized to the levels of total $p22^{phox}$ detected in the same samples. *$p$<0.05 for indicated values versus vehicle values under the same gene transfection. †P<0.05 for indicated values versus WT TNFα values. n=4 independent experiments.

**Figure 5.** TNFα-induced $p47^{phox}$ membrane translocation and binding to $p22^{phox}$, redox signaling and cell apoptosis in HMEC. (A) Western blot. The optical densities (OD) of protein bands were quantified and normalized to the levels of CD31 (an endothelial membrane marker) detected in the same samples. (B) $p47^{phox}$ was immunoprecipitated (IP) and detected by Western blot for the presence of $p22^{phox}$ and $p47^{phox}$ phosphorylation (P-p47). The optical densities (OD) of protein bands were quantified and normalized to the levels of total $p47^{phox}$ (T-p47) detected in the same samples. (C) Western blots. The phospho-bands were quantified and normalized to the total levels of the same protein detected in the same samples. (D) Right panels: Annexin-V/propidium iodide detection of cell apoptosis (upper right square) by flow cytometry. Apoptotic cells were presented as a percentage of total cells (20,000). *$p$<0.05 for indicated value versus vehicle values under the same gene transfection. †$p$<0.05 for indicated values versus WTp22 TNFα values. n=4 independent experiments.

**Figure 6.** TNFα-induced NFκB nuclear translocation, VCAM1 expression and monocyte adherence in HPMECs. (A) Immunofluorescence microscopy detection of NFkB (green) nuclear translocation and VCAM1 (red) expression. Nuclei were labelled with DAPI (blue) to visualize cells. The fluorescence intensity was quantified from 20 images/per group. n=3 independent experiments. (B) Flow cytometry detection of VCAM-1 expression. (C) U937 monocytes were labeled with FITC (green) and the number of monocytes adhering to the HPMEC monolayer was counted for quantification. *$p$<0.05 for indicated value versus vehicle values under the same gene transfection. †$p$<0.05 for indicated values versus WTp22 TNFα values. n=4 independent experiments (B-C) .

**Figure 7.** Experiments using $p22^{phoxdepl}$ HeLa cells. (A) Western blots. Optical densities (OD) of protein bands were quantified and normalized to the levels of α-tubulin detected in the same sample. (B) Immunofluorescence detection of $p22^{phox}$ expression. The color images and quantification of $p22^{phox}$ fluorescence intensities are presented in the Supplemental Figure 7. (C) Flow cytometry detection of anti-Nox2 antibody (7D5) binding to HeLa cells. Shaded area represents control cells without Nox2 antibody labelling. (D) $O_2^{\cdot -}$ production. SCR: scrambled shRNA. *$p$<0.05 for indicated values versus SCR values under the same treatment. †$p$<0.05 for indicated values versus WTp22 values under the same treatment. n=4 independent experiment.

**Figure 8.** The effects of C242T $p22^{phox}$ SNP on Nox2 expression and high-glucose induced ROS production in human saphenous veins. (A) Genotyping of C242T $p22^{phox}$ SNP (left panel) and calculated frequency in a total of 36 samples. WT $p22^{phox}$ appeared as a single band of 348 bp and C242T SNP had two bands at 188 and 160 bp. B) Nox2 expression detected by dot-blotting. C) 3NT formation detected by dot-blotting. *$p$<0.05 for indicated values versus CC values. D) Nox2 (red color) expression detected by Immunofluorescence. Lumen was labeled for the location of the endothelium. Vessel structure was shown by H&E staining (right panel). E) Left panels: Representative images of vessel ROS production with or without high-glucose (H-glucose) challenge (24 h) detected by DHE fluorescence on vessel sections. Superoxide dismutase (SOD) was used to confirm the detection of $O_2^{\cdot -}$. *$p$<0.05 for indicated values versus control values in the same genetic group. †$p$<0.05 for indicated values versus CT values under H-glucose.

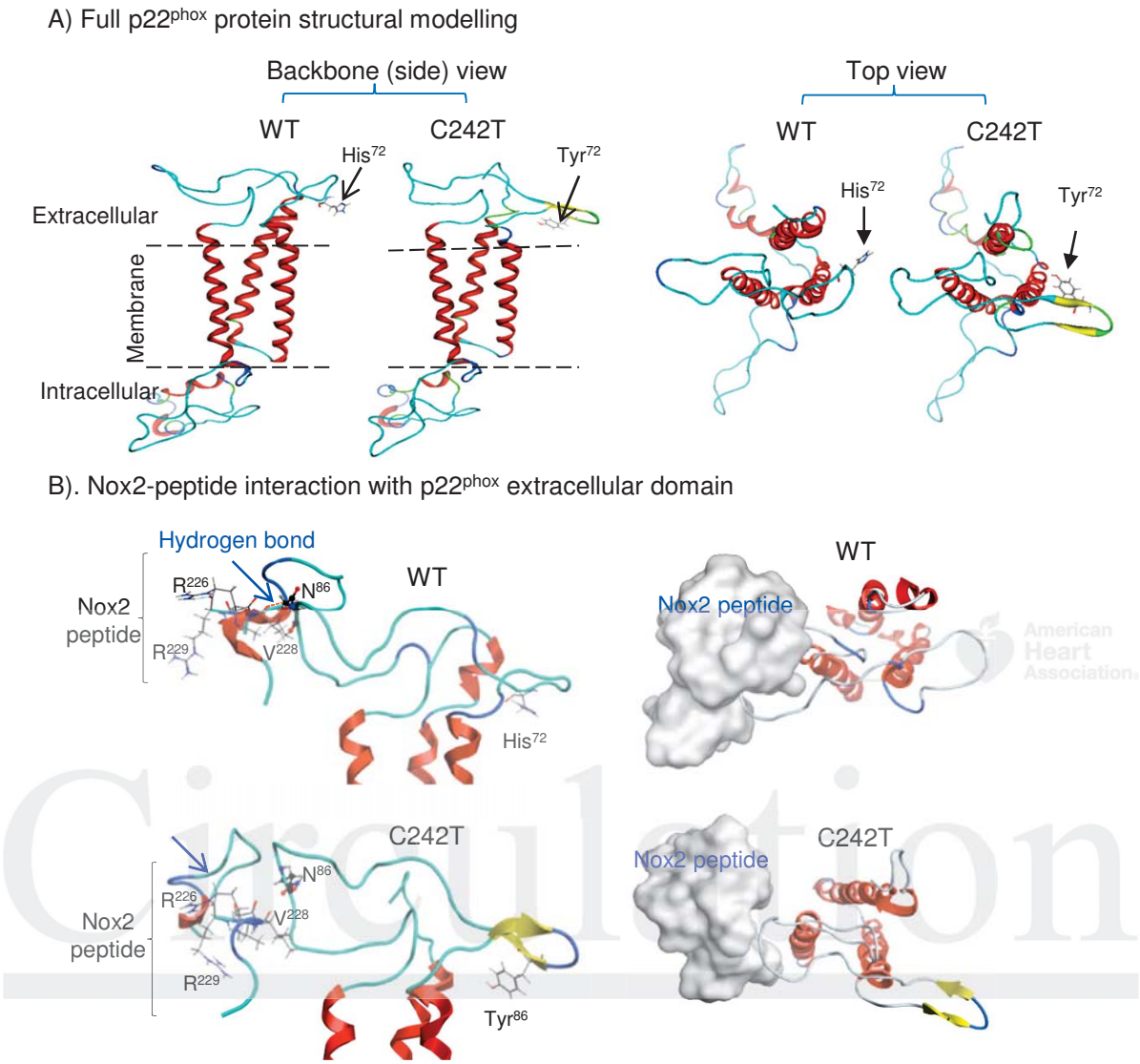


Figure 1

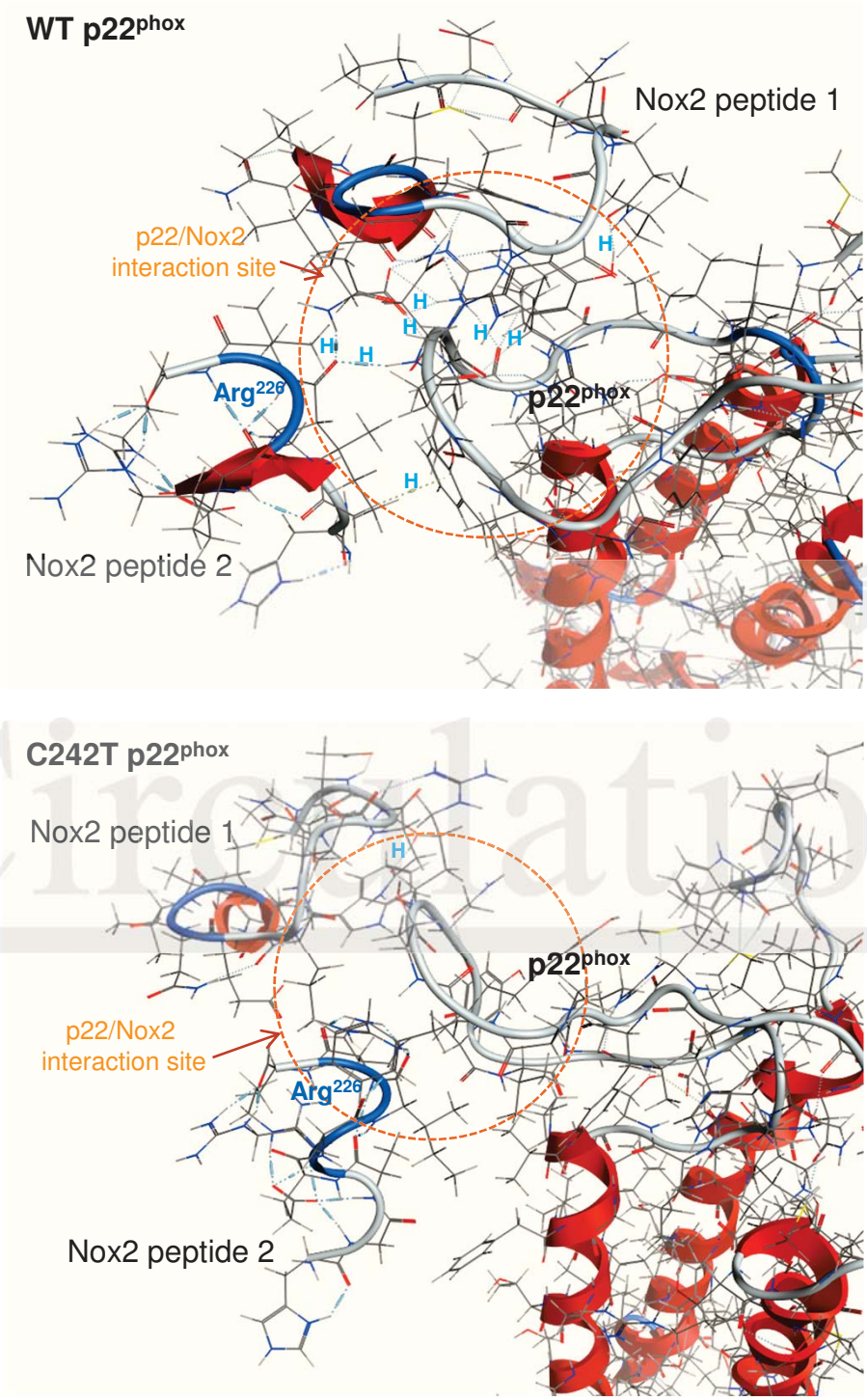


Figure 2

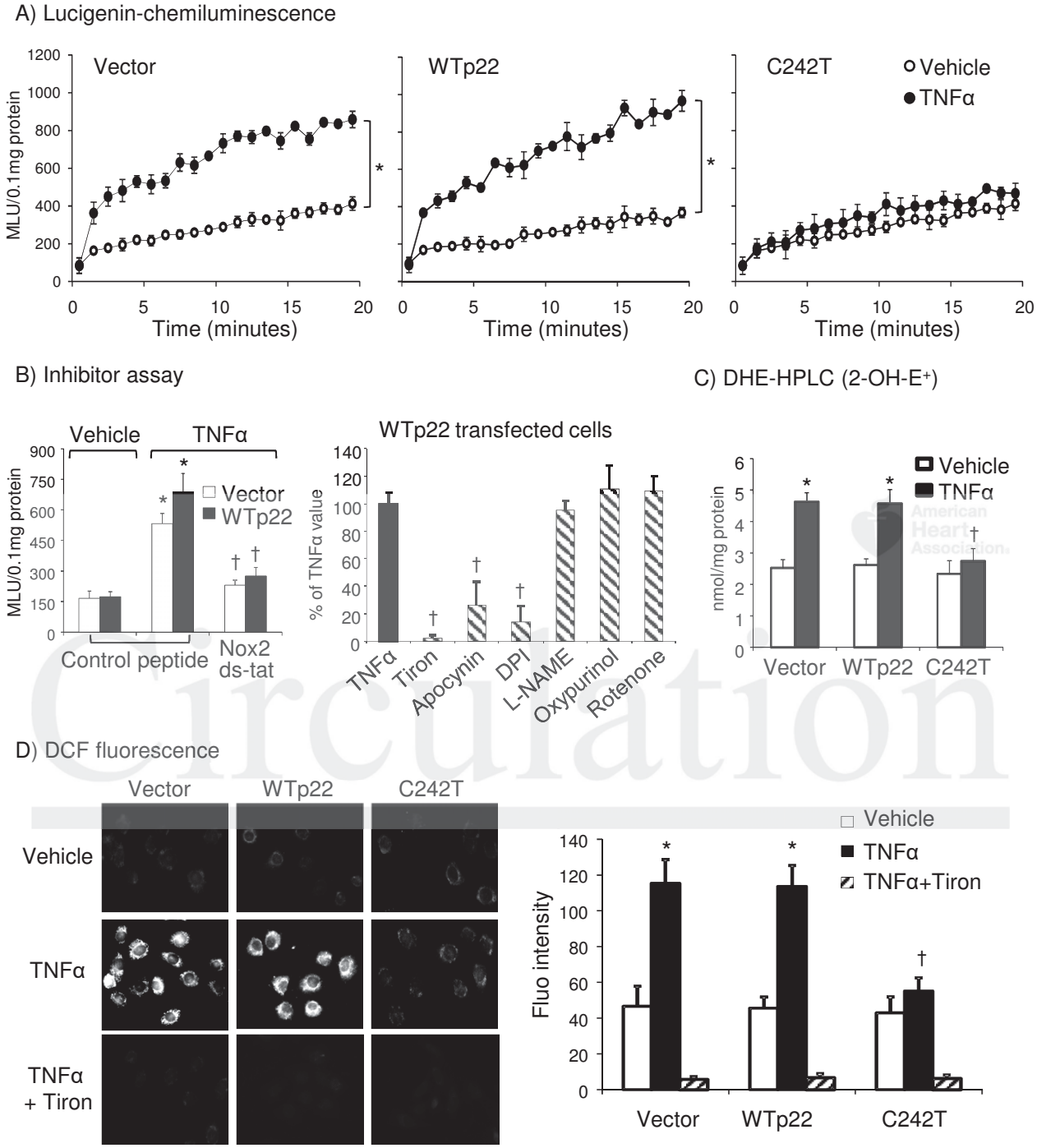


Figure 3

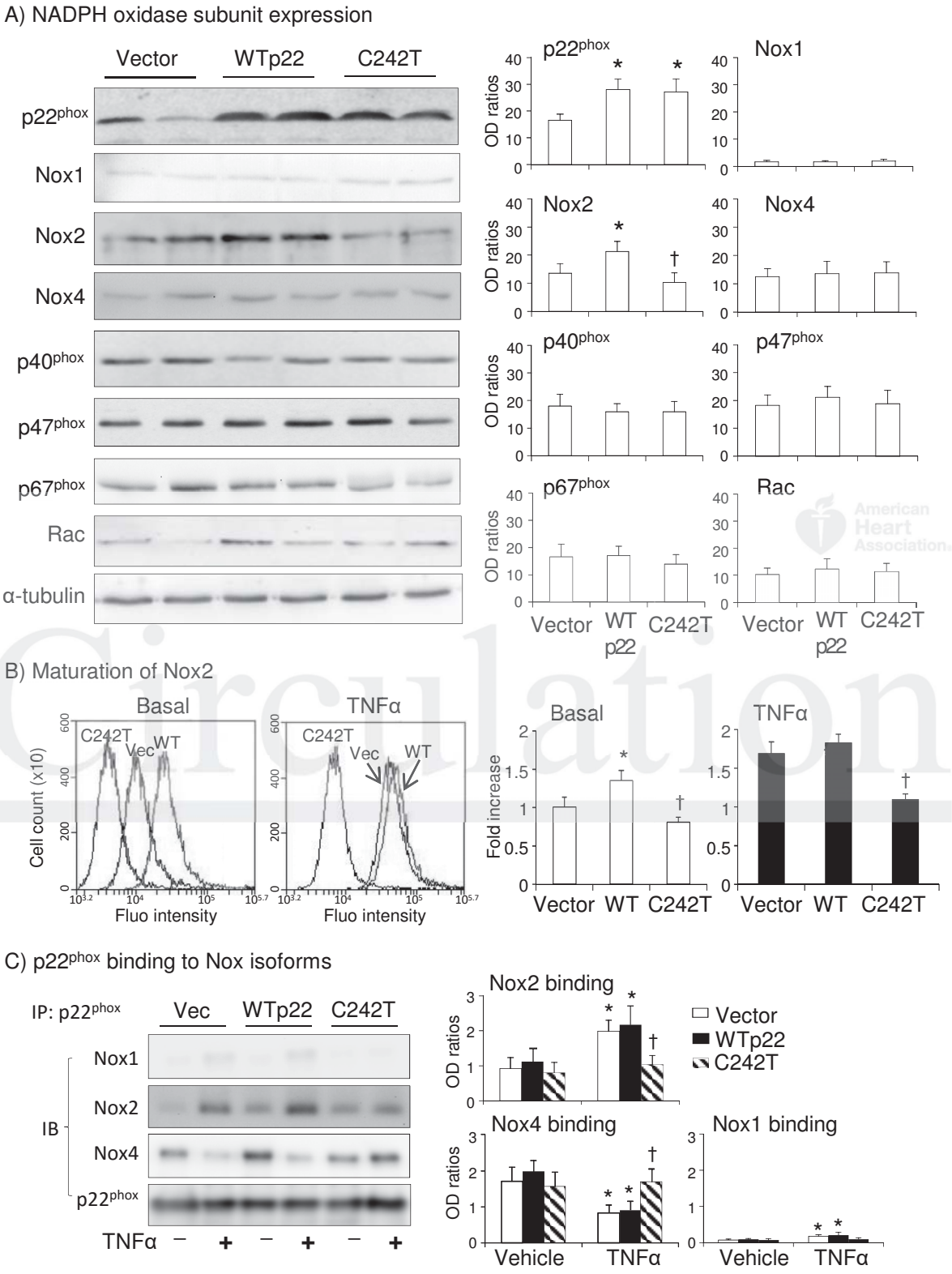


Figure 4

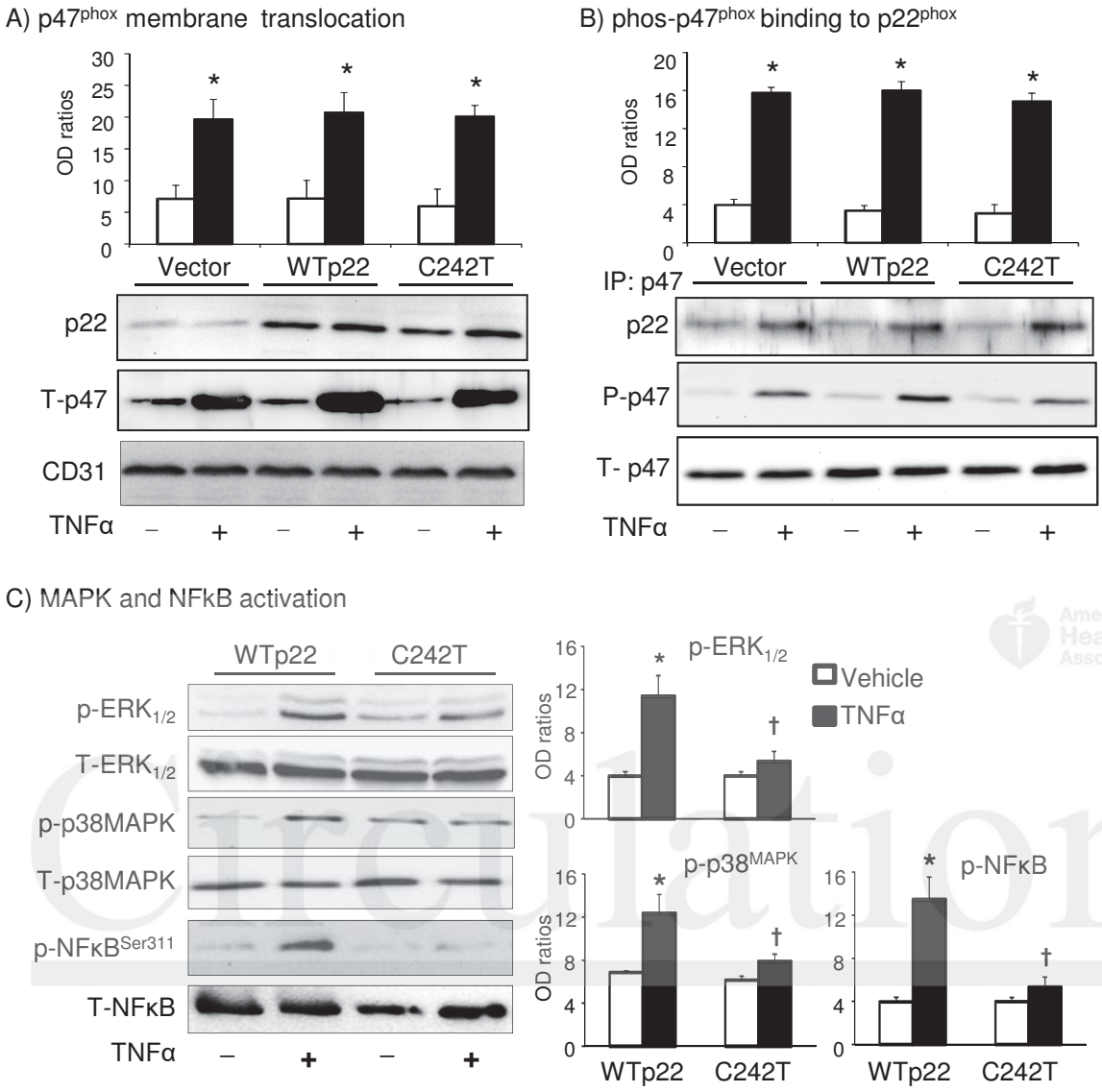


Figure 5

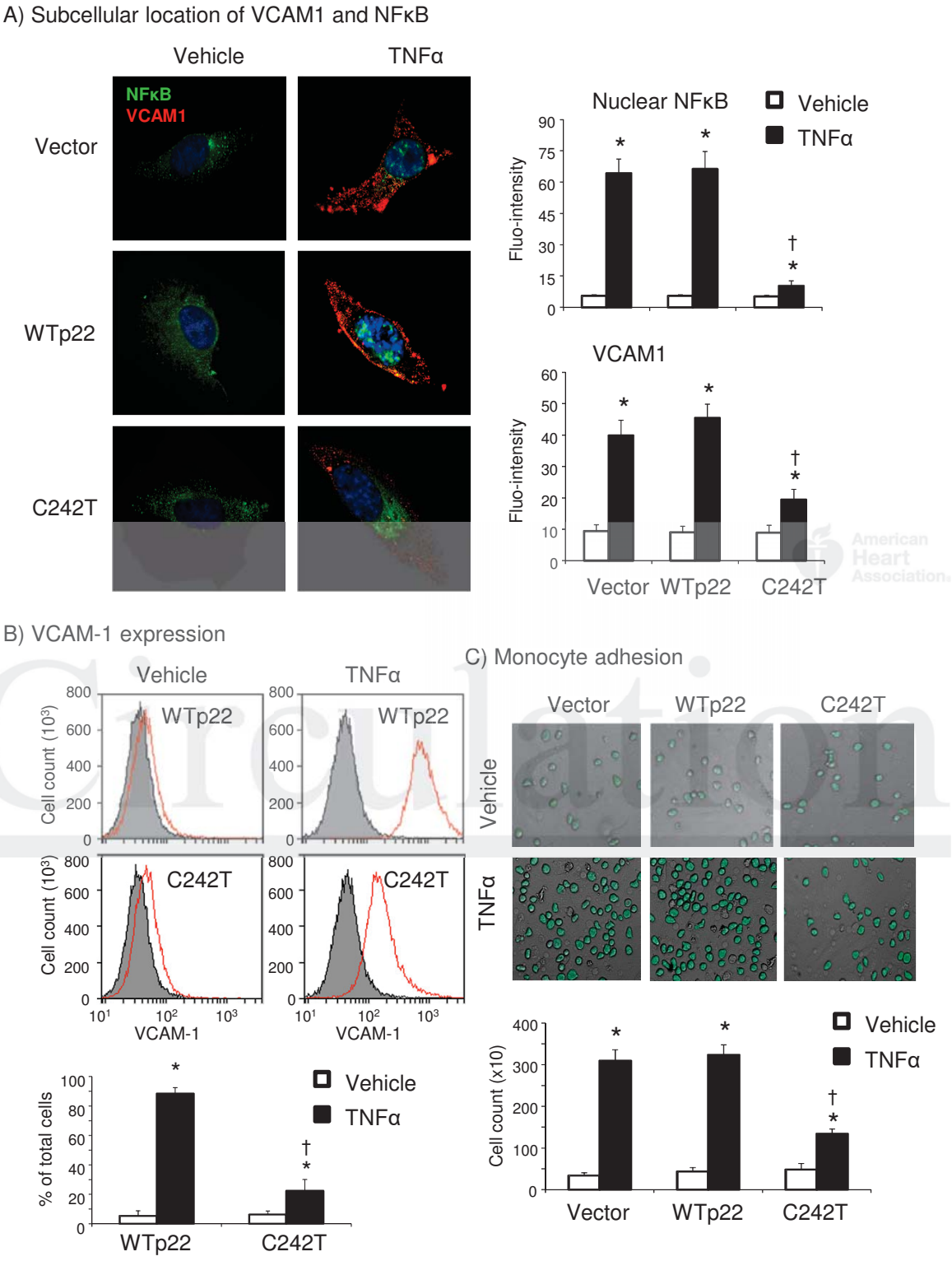


Figure 6

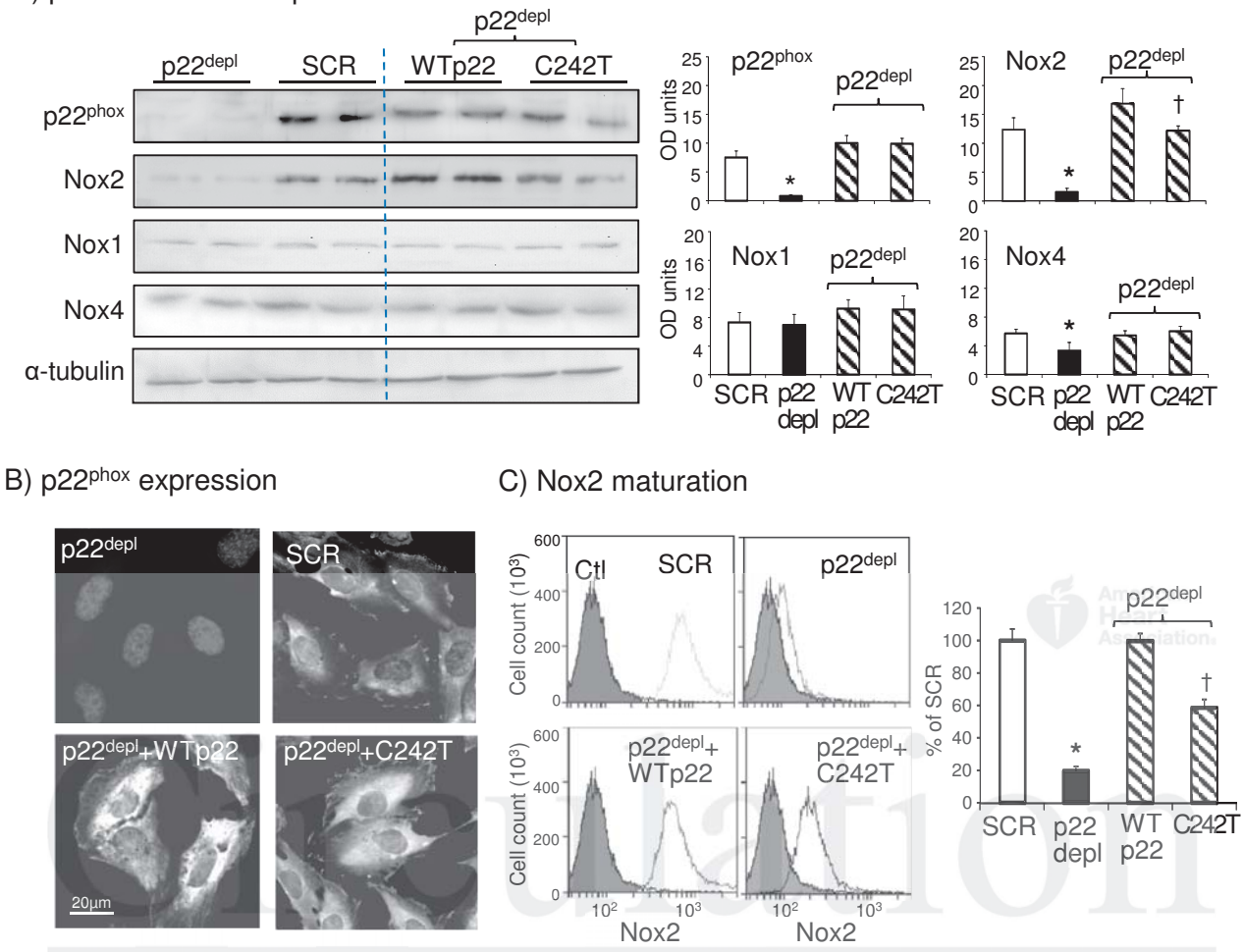


Figure 7

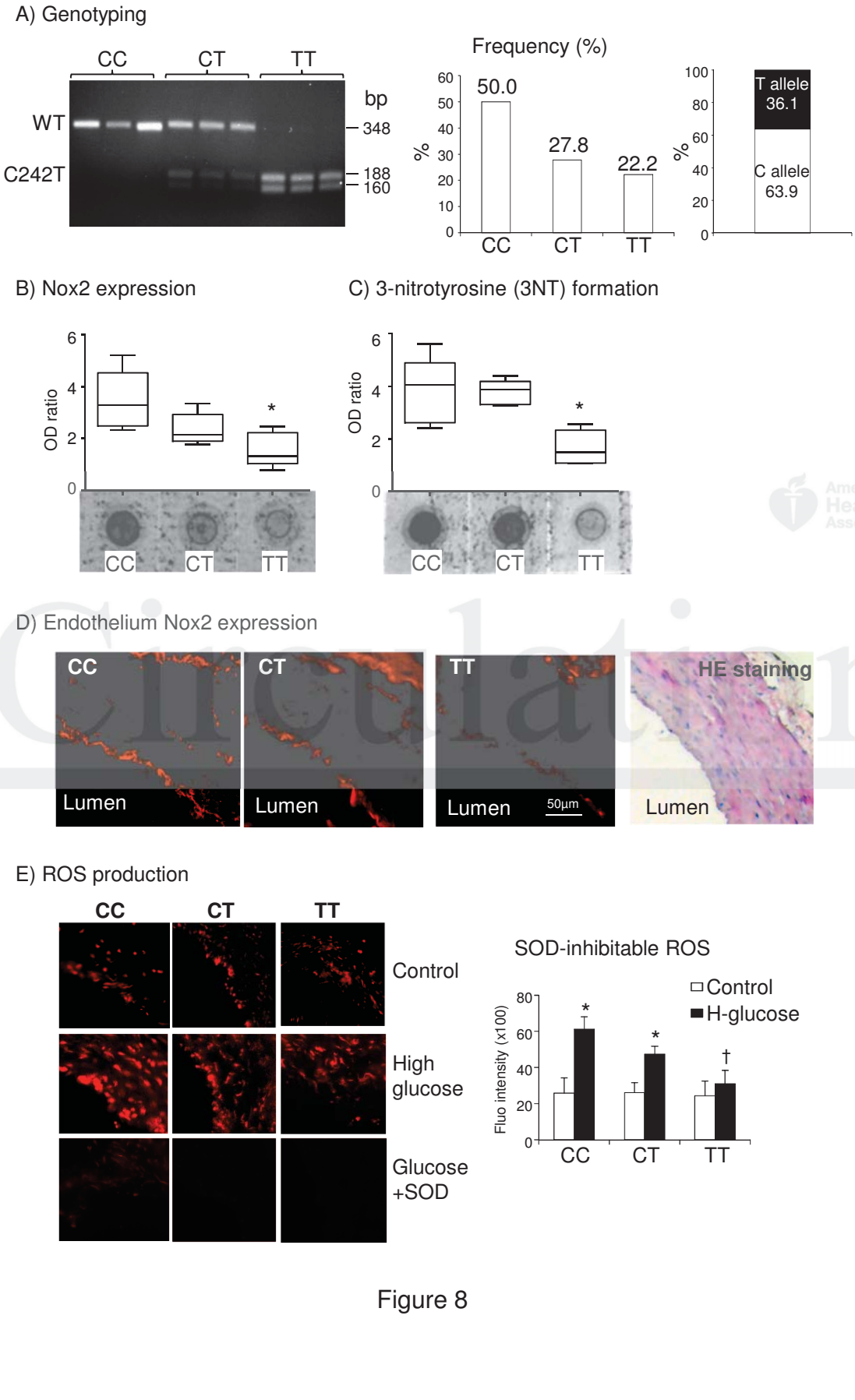


Figure 8

# p22$^{phox}$ C242T SNP Inhibits Inflammatory Oxidative Damage to Endothelial Cells and Vessels

Daniel N. Meijles, Lampson M. Fan, Maziah M. Ghazaly, Brendan Howlin, Martin Krönke, Gavin Brooks and Jian-Mei Li

*Circulation.* published online May 9, 2016;
*Circulation* is published by the American Heart Association, 7272 Greenville Avenue, Dallas, TX 75231

Print ISSN: 0009-7322. Online ISSN: 1524-4539

# SUPPLEMENTAL MATERIAL

## Materials and methods

*Reagents*

Human recombinant TNFα was from Roche Applied Sciences. Polyethyleneimine (linear MW=25,000) was from Polysciences Inc (UK). Rabbit and goat polyclonal antibodies to NADPH oxidase subunits Nox1, Nox2, Nox4, $p22^{phox}$, $p47^{phox}$, $p67^{phox}$, rac1, total ERK1/2, p38 MAPK, total JNK, NFκB, phosphor-$NF\kappa B^{Ser311}$, CD31 and α-tubulin were purchased from Santa Cruz (UK). Monoclonal antibody to $p40^{phox}$ was from Upstate Biotechnology. Antibodies to phospho-ERK1/2, phospho-p38 MAPK, phospho-JNK were from Cell Signalling Technology. Dihydroethidium (DHE) and 5-(and 6)-chloromethyl-2',7'-dichlorodihydrofluorescein diacetate (DCF) were from Invitrogen. Other reagents were from Sigma except where specified.

*In silico protein structural modelling and protein docking*

The *in silico* model of $p22^{phox}$ was generated as reported previously by incorporating data from the online prediction servers with the molecular operating environment (MOE; Chemical Computing Group Inc., Canada) and subjected to energy minimization using the AMBER99 force field until all unfavorable residue contacts and atom clashes were repaired as described previously[1,2]. To calculate differences in the WT and C242T extracellular domains, the root-mean squared deviation (RMSD) was investigated by superimposing alpha-carbon backbone atoms in MOE, expressed in angstroms (Å) as described previously[1, 2]. RMSD results were collected from three independent modeling experiments and expressed as Mean±SD of 3 sets of data. The docking of $p22^{phox}$ with Nox2 peptide was performed in the MOE program and refined by energy minimization using the AMBER99 forcefield as described previously[2].

*HapMap analysis of the CYBA gene*

Using the International HapMap Project (HapMap phase II+III; dbSNP b126), 6 common *CYBA* SNPs were chosen from the National Centre for Biotechnology Information (NCBI) SNP database (dbSNP). Haplotype association was calculated using the Haplo-view analysis program (version 4.2) in the northern and western European population (CEU) and is expressed as $r^2$. *CYBA* SNPs in complete linkage disequilibrium have an $r^2$ correclation value of 100%.

*Site-directed mutagenesis*

The recombinant human $p22^{phox}$ cDNA sequence (GenBank:BC006465.1) subcloned into pcDNA3.1 (Invitrogen) at Xba I and Hind III sites was a kind gift from Prof. J.D. Lambeth (Emory University, USA). Primer design and the site-directed mutagenesis experiments were performed according to the manufacturer's instruction using the QuikChange Multi Site-Directed Mutagenesis kit (Agilent Technologies) as described previously[3]. The PCR products of these mutations were cloned into E.coli, DH5α (Invitrogen), and the C242T substitution of the $p22^{phox}$ was verified by molecular sequencing.

*Cell culture, Gene transfection and TNFα stimulation*

Human pulmonary microvascular endothelial cells (HPMEC-ST1.6R) were a kind gift from Dr R. Unger (Johannes Gutenberg University, Germany)[4] and were cultured in M199 medium containing 10% (v/v) fetal bovine serum (FBS), 20µg/ml of endothelial cell growth supplement (ECGS) and 25µg/mL heparin. The monocytic cell line (U937) was obtained from ATCC and grown in RPMI medium supplemented with 10% (v/v) FBS, 2mmol/L L-glutamine, 100U/mL penicillin and 100µg/mL streptomycin. CMEC were isolated from the hearts of 10-12 week old Nox2 KO and WT mice and cultured as described previously and used at passage 2[5,6]. The shRNA $p22^{phox}$ targeted sequence is: GGCCCTTTACCAGGAATTA, and the shRNA scrambled control sequence is GACAACGTATCCGTCAGTT. The shRNA $p22^{phox}$ ($p22^{phox\text{-}depl}$) and shRNA scrambled control HeLa cells were generated using the techniques as described previously[7] in the laboratory of Professor Krönke (University of Cologne, Germany). Gene transfection was performed exactly as described previously using polyethyleneimine[3]. Transfection efficiency (65-70%) was verified with a reporter gene, β-galactosidase[3]. After 48h of culture, cells were treated with either vehicle or TNFα (100 U/mL) for 30 min or 24 h according to the experimental design in 5% FCS/DMEM and harvested for further experiments.

*Preparation of cell membrane fraction*

Cellular membrane protein fraction was prepared as described previously [8]. Briefly, cells were detached by mechanical scraping and then were re-suspended in MOPS-KOH buffer (MOPS-KOH 20mmol/L, sucrose 250mmol/L, pH 7.4). Cell homogenate was quickly centrifuged at 1,475g for 15 min. to remove any unbroken cells and the nuclei-enriched fraction. The resulting supernatant was then centrifuged for 15 min. at 29,000g to pellet mitochondria and subcellular organelles. The resulting supernatant was centrifuged for 60

min. at 100,000g to produce a membrane fraction. Pellets of the membrane fraction were re-suspended in homogenization buffer and washed once before using.

*Human saphenous vein sample collection, genotyping and glucose challenge.*

Segments of human saphenous vein were collected from 36 patients (without histories of coronary heart diseases) undergoing phlebectomies at a specialist vein unit. Informed consent was obtained from the patients and the project was approved by the local NHS and the University ethical committees. Vein segments (3-5 mm long) with normal morphological appearance were used for the experiments. The C to T substitution at 242 in the CYBA coding sequence was examined exactly as described previously using specific intron-spanning primers (forward: 5'CGCTGGCGTCCGGCCTGATCCTCA3'; reverse: 5'ACGCACAGCCGCCAGTAGGTAGAT3')[9]. Expression of the T-allele produces two bands at 160- and 188-bp respectively, whereas the C-allele has one band at 348-bp. For the experiments of high-glucose challenge, vessel segments were then cultured in the 5% FCS/M199 medium with normal glucose (5 mmol/L) or high glucose (25 mmol/L) for 24 h before ROS measurement.

*Measurement of ROS production*

Endothelial (or vessel tissue) $O_2^{\cdot-}$ production was measured using four independent methods as described previously[10]. 1) Lucigenin (5μmol/L)-chemiluminescence (BMG Lumistar, Germany). The assay specificity for $O_2^{\cdot-}$ detection was confirmed by adding tiron (10mM), a non-enzymatic scavenger of $O_2^{\cdot-}$. Potential enzymatic sources of $O_2^{\cdot-}$ production were also investigated by using the following inhibitors: Nox2 –ds-tat (10 μmol/L), apocynin (100μmol/L), N-ω-nitro-L-arginine methyl ester (L-NAME, 100μmol/L), rotenone (50μmol/L), oxypurinol (100μmol/L) or diphenyleneiodonium (DPI, 20μmol/L). 2) DHE fluorescence HPLC assay with or without superoxide dismutase–polyethylene glycol (PEG-SOD) was performed exactly as described previously[3, 11]. The amount of 2-OH-E generated was normalized to the protein concentration of the same sample. 3) The intracellular $O_2^{\cdot-}$ production was examined using DHE flow cytometry in the presence or absence of tiron. 4) The ROS production by adherent cells was measured using DCF fluorescence acquired under Olympus BX61 fluorescence microscopy. Fluorescence intensity was quantified from at least 3 random fields (269.7 x 269.2 μm) per chamber, >100 cells were assessed per cell culture experiment, and at least 3 separate cell cultures per condition[3].

*Amplex Red assay for $H_2O_2$ measurement*

Total cell homogenate $H_2O_2$ production was measured using the Amplex Red (Invitrogen Inc.) assay as described previously[12]. Briefly, 50 µg/ml protein was added to the wells of a black 96-well plate containing the assay buffer (25 mmol/L HEPES, pH 7.4, containing 0.12 mol/L NaCl, 3 mmol/L KCl, 1 mmol/L MgCl2, 0.1 mmol/L Amplex red, and 0.32 U/ml HRP). The reaction was initiated by the addition of 36 µmol/L NADPH and detected using a BMG Fluostar Galaxy multimode microplate reader. Catalase (300 U/ml) was added in the parallel wells. $H_2O_2$ production was quantified against a standard curve.

*Quantitative real-time (RT)-PCR*

These experiments were performed as described previously[13] using human primers for Nox1 (F: CAGGGAGACAGGTGCCTTTTCC; R: GAACCAGAGCAGTCCAAACTCG), Nox2 (F: CAAGATGCGTGGAAACTACCTAAGAT; R: TCCCTGCTCCCACTAACATCA) and Nox4 (F: CTGCTGACGTTGCATGTTTC; R: TTCTGAGAGCTGGTTCGGTT), β-actin, (F: CTGGCACCCAGCACAATG; R: GCCGATCCACACGGAGTACT). Each gene expression levels were normalized to β-actin, and expressed log2 ratio of ΔCt values.

*Immunoprecipitation and immunoblotting*

Immunoblotting experiments were performed exactly as described previously [6]. The α-tubulin detected in the same sample was used as a loading control. Co-immunoprecipitation (IP) was performed as described previously using anti-$p22^{phox}$ or anti-$p47^{phox}$ antibody coated protein G agarose beads[14]. Normal rabbit IgG-coupled beads were used as negative controls. Samples were then examined for the presence of other Nox subunits pulled down by the beads using immunoblotting (IB). The levels of total $p22^{phox}$ or total $p47^{phox}$ in the same IP sample were used as loading controls.

*Dot blotting*

Human vessel Nox2 expression and protein nitration were detected by dot-blot analysis according to a previous publication[15] using 5 µl (50 µg) of protein samples. Immuno-blotting was performed using specific antibodies to Nox2 or 3-nitrotyrosine (3NT). Positive labelling was detected by fluorescence (Cy5 or FITC)-conjugated secondary antibodies. Blots were scanned using a fluorescence imager (Typhoon Trio, Amersham) and quantified.

*Flow cytometry*

This was done exactly as described previously[16]. Briefly, cells were trypsinized, washed in PBS supplemented with 1% BSA and 1% FCS. Cells were then incubated on ice for 30 min with primary antibodies (as indicated in the text) or buffer only as controls. After washing, cells were then incubated with FITC- or Cy3-labelled specific secondary antibodies. Fluorescence intensity of cells was measured using Accuri C6 flow cytometer (BD Bioscience). Data were analyzed with the Accuri C6 software.

*Immunofluorescence microscopy*

Cell preparation and immunofluorescence microscopy were performed as described previously[8]. Cells were labelled with primary antibodies and detected using biotin-conjugated anti-rabbit or anti-goat IgG (1:1000 dilution) as the secondary antibodies. Specific antibody binding was detected by extravidin-FITC (green) or streptavidin-Cy3 (red). Normal rabbit or goat IgG (5μg/mL) was used in place of primary antibody as negative controls. Images were acquired with an Olympus BX61 fluorescence microscope system. Fluorescence intensities were quantified as described above.

*Statistics*

Data were presented as means ± SD of results taken from at least 3 independent cell cultures and gene transfections for each condition. In the case of CMEC, each isolation used 6 mice/per group, and the data presented were the means ± SD from at least 3 separate CMEC isolations. Comparisons were made by ANOVA with Bonferroni test analysis except where it was specified in the figure legend. $P<0.05$ was considered statistically significant.

**Supplemental Table I.**

Differences in the trans-membrane domain sequences (300 amino acids) between Nox2 and Nox1.

```
Nox2:       1-MGNWAVNEGLSIFVILVWLGLNVFLFVWYYRVYDIPPKFFYTRKLLGSALALARAPAACL
Nox1:       1-MGNWVVNHWFSVLFLVVWLGLNVFLFVDAFLKYEKADKYYYTRKILGSTLACARASALCL

Nox2:      61-NFNCMLILLPVCRNLLSFLRGSSACCSTRVRRQLDRNLTFHKMVAWMIALHSAIHTIAHL
Nox1:      61-NFNSTLILLPVCRNLLSFLRGTCSFCSRTLRKQLDHNLTFHKLVAYMICLHTAIHIIAHL

Nox2:     121-FNVEWCVNARVNNSDPYSVALSELGDRQNESYLNFARKRIKNPEGGLYLAVTLLAGITGV
Nox1:     121-FNFDCYSRSRQATDGSLASILSSLSHDEKKGGSWLNPIQSRNTTVEYVTFTSIAGLTGVI

Nox2:     181-VITLCLILIITSSTKTIRRSYFEVFWYTHHLFVIFFIGLAIHGAERIVRGQTAESLAVHN
Nox1:     181-MTIALILMVTSATEFIRRSYFEVFWYTHHLFIFYILGLGIHGIGGIVRGQTEESMNESHP

Nox2:     241-ITVCEQKISEWGKIKECPIPQFAGNPPMTWKWIVGPMFLYLCERLVRFWRSQQKVVITKV
Nox1:     241-RKCAESFEMWDDRDSHCRRPKFEGHPPESWKWILAPVILYICERILRFYRSQQKVVITKV
```

Two epitopes (yellow colour shaded areas, epitope 1: 160-INKP-163 and epitope 2: 226-RIVRG-230) in the extracellular region of Nox2 are found to be involved in the interaction with $p22^{phox}$ (details in Figure 2), and are recognised by antibody 7D5. Sequence homology matching table shows that Nox1 does not contain the sequence of epitope 1. In the sequence of epitope 2, the key positively charged amino acid ($Arg^{226}$) of Nox2 that forms the crucial hydrogen bond with $Asn^{86}$ of $p22^{phox}$ (see Figure 2) is substituted by the smallest and uncharged amino acid ($Gly^{225}$) in Nox1.

**References:**


(1) Meijles D, Howlin BJ, Li J-M. Consensus in silico computational modelling of the $p22^{phox}$ subunit of the NADPH oxidase. *Comput Biol Chem* 2012;39:6-13.

(2) Meijles DN, Fan LM, Howlin BJ, Li JM. Molecular insights of p47phox phosphorylation dynamics in the regulation of NADPH oxidase activation and superoxide production. *J Biol Chem* 2014;289:22759-70.

(3) Teng L, Fan LM, Meijles D, Li J-M. Divergent effects of $p47^{phox}$ phosphorylation at S303-4 or S379 on tumor necrosis factor-a signaling via TRAF4 and MAPK in endothelial cells. *Arterioscler Thromb Vasc Biol* 2012;32:1488-96.

(4) Unger RE, Krump-Konvalinkova V, Peters K, Kirkpatrick CJ. In vitro expression of the endothelial phenotype: Comparative study of primary isolated cells and cell lines, including the novel cell line HPMEC-ST1.6R. *Microvascular Res* 2002;64:384-97.

(5) Li J-M, Mullen AM, Shah AM. Phenotypic properties and characteristics of superoxide production by mouse coronary microvascular endothelial cells. *J Mol Cell Cardiol* 2001;33:1119-31.

(6) Fan LM, Teng L, Li J-M. Knockout of $p47^{phox}$ uncovers a critical role of $p40^{phox}$ in reactive oxygen species production in microvascular endothelial cells. *Arterioscler Thromb Vasc Biol* 2009;29:1651-6.

(7) Yazdanpanah B, Wiegmann K, Tchikov V, Krut O, Pongratz C, Schramm M, Kleinridders A, Wunderlich T, Kashkar H, Utermohlen O, Bruning JC, Schutze S, Kronke M. Roboflavin kinase couples TNF receptor 1 to NADPH oxidase. *Nature* 2012;460:1159-63.

(8) Li J-M, Fan LM, Christie MR, Shah AM. Acute tumor necrosis factor alpha signaling via NADPH oxidase in microvascular endothelial cells: role of $p47^{phox}$ phosphorylation and binding to TRAF4. *Mol Cell Biol* 2005;25:2320-30.

(9) Guzik TJ, West NEJ, Black E, McDonald D, Ratnatunga C, Pillai R, Channon KM.. Functional effect of the C242T polymorphism in the NAD(P)H oxidase p22phox gene on vascular superoxide production in atherosclerosis. *Circulation* 2000;102:1744-7.

(10) Fan LM, Li JM. Evaluation of methods of detecting cell reactive oxygen species production for drug screening and cell cycle studies. *J Pharmacol Toxicol Methods* 2014;8;70:40-7.

(11) Fan LM, Douglas G, Bendall JK, McNeill E, Crabtree MJ, Hale AB, Mai A, Li JM, McAteer MA, Schneider JE, Choudhury RP, Channon KM. Endothelial Cell-Specific ROS Production Increases Susceptibility to Aortic Dissection. *Circulation* 2014;129:2661-72.

(12) Csanyi G, Yao M, Rodriguez AI, Al Ghouleh, I, Sharifi-Sanjani M, Frazziano G, Huang X, Kelley EE., Isenberg JS, and Pagano PJ. Thrombospondin-1 regulates blood flow via CD47 receptor-mediated activation of NADPH oxidase 1. *Arterioscler Thromb Vasc Biol* 2012;32:2966-73.

(13) Li J-M, Fan LM, George VT, Brooks G. Nox2 regulates endothelial cell cycle arrest and apoptosis via $p21^{cip1}$ and p53. *Free Radic Biol Med* 2007;43:976-86.

(14) Li J-M, Shah AM. Intracellular localization and preassembly of the NADPH oxidase complex in cultured endothelial cells. *J Biol Chem* 2002;277:19952-60.

(15) Knorr M, Hausding M, Kroller-Schuhmacher S, Steven S, Oelze M, Heeren T, Scholz A, Gori T, Wenzel P, Schulz E, Daiber A, Munzel T. Nitroglycerin-induced endothelial dysfunction and tolerance involve adverse phosphorylation and S-Glutathionylation of endothelial nitric oxide synthase: beneficial effects of therapy with the AT1 receptor blocker telmisartan. *Arterioscler Thromb Vasc Biol* 2011;31:2223-31.

(16) von Lõhneysen K, Noack D, Wood MR, Friedman JS, Knaus UG. Structure insights into Nox4 and Nox2: motifs involved in function and cellular localization. *Mol Cell Biol* 2010;30:961-75.

**Supplemental Figure I:** Inhibition of TNFα-induced $O_2^{\cdot-}$ production by human coronary arterial endothelial cells (HCAEC) using specific peptide inhibitors to Nox1 and Nox2.

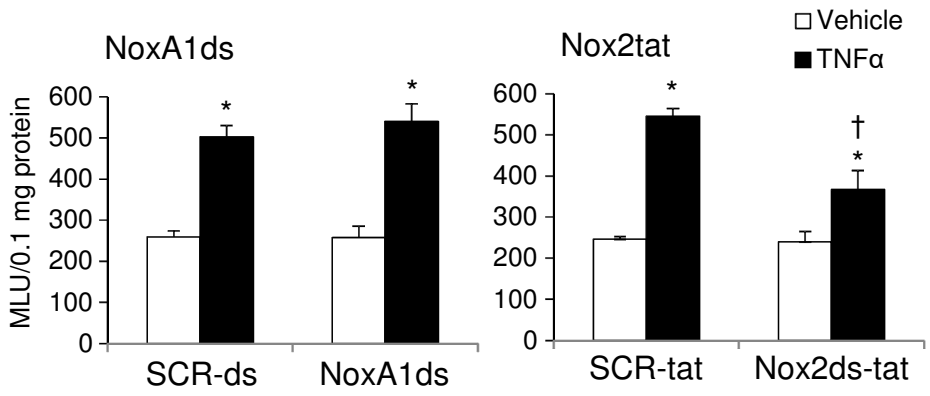


HCAEC were cultured in the complete culture medium. Peptides (10 µmol/L) were added into the culture medium 1 h before TNFα stimulation. Cells were then stimulated by TNFα (100 U/ml) for 30 min. NADPH-dependent $O_2^{\cdot-}$ production by cell homogenates was measured by lucigenin (5 µmol/L)-chemiluminescence. *$p$<0.05 for indicated values versus vehicle values in the same peptide treatment group. †$p$<0.05 for indicated values versus TNFα values in the scrambled peptide (SCR-tat) treatement group. n=4 separate experiments.

**Supplemental Figure II:** Nox4-derived $H_2O_2$ production by HEK293 cells co-transfected with Nox4 plus WT or C242T $p22^{phox}$

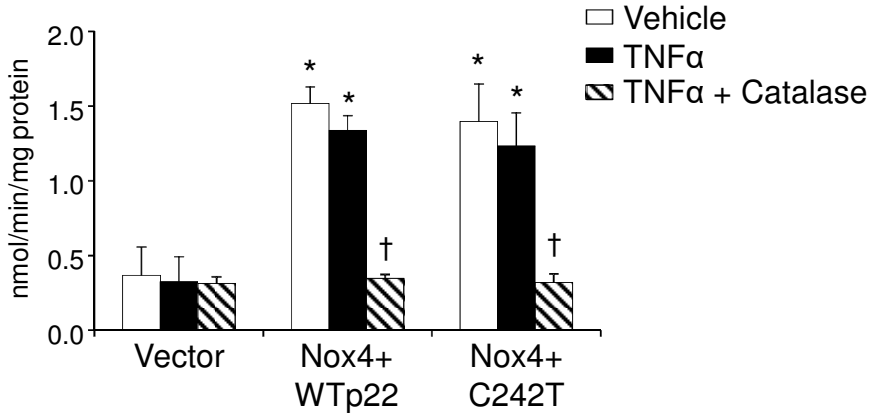


HEK293 cells were co-transfected with human Nox4 plus either WT or C242T $p22^{phox}$ plasmids. Cells were then stimulated with or without TNFα for 30 min. The $H_2O_2$ production was measured in cell homogenates by Amplex-red assay in the presence or absence of catalase (300 units/ml). *P<0.05 for indicated values versus vector values under the same treatment. †$p$<0.05 for catalase values versus vehicle or TNFα value in the same gene transfection group. n=4 separate gene transfection experiments.

**Supplemental Figure III:** Representative examples of Western blots of co-immunoprecipitatiion (used in Figure 3C).

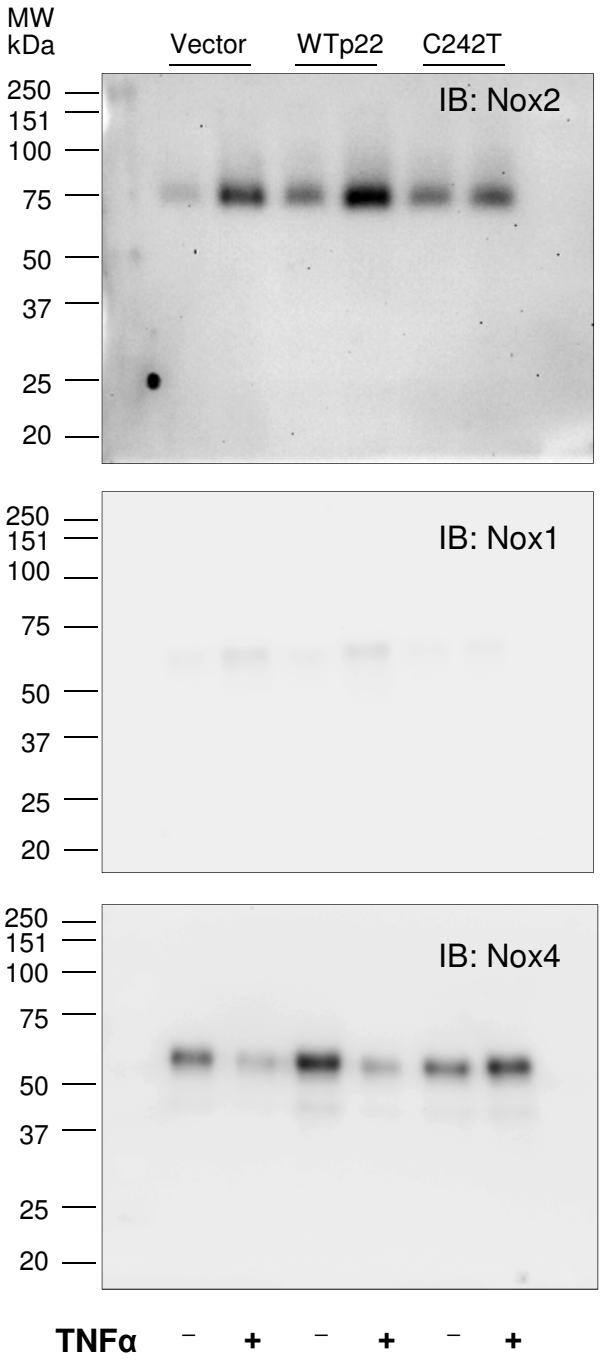


$p22^{phox}$ was immunoprecipitated (IP) and detected by immunoblotting (IB) for the existence (pulled-down) of Nox2, Nox1 and Nox4 (in Figure 3C). The molecular weights are indicated on the left.

**Supplemental Figure IV.** The effect of C242T p22$^{phox}$ on TNFα-induced Nox2 and Nox4 protein expression in HPMEC (Input data for Figure 4C).

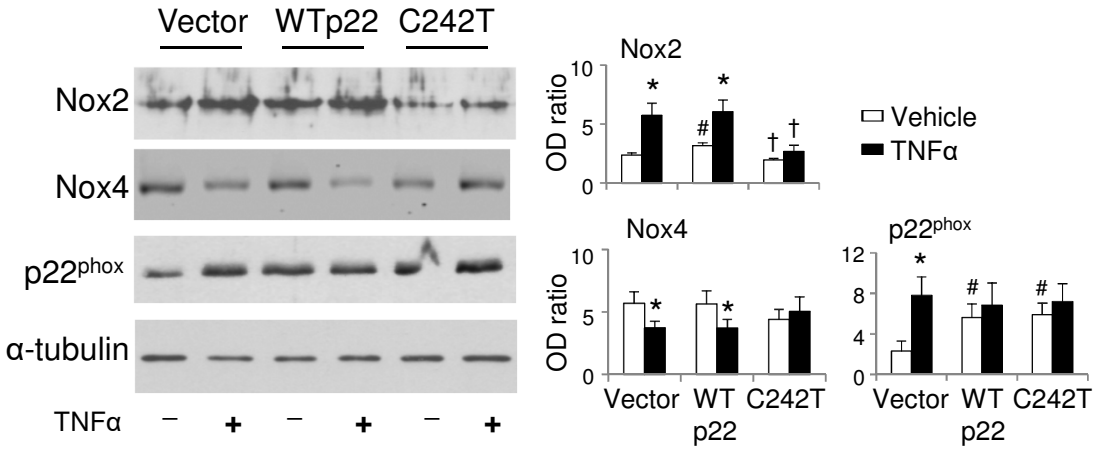


The whole cell homogenates were used for Western blots. Optical density of protein bands were quantified and normalized to α-tubulin detected in the same sample. *$p$<0.05 for TNFα values versus vehicle values in the same gene transfection group. †$p$<0.05 for indicated values versus WT TNFα values. #$p$<0.05 for indicated values versus vector vehicle values. n=4 separate gene transfection experiments.

**Supplemental Figure V.** Effects of p22$^{phox}$ C242T SNP on TNFα -induced $O_{2}^{\cdot -}$ production by endothelial membrane fractions

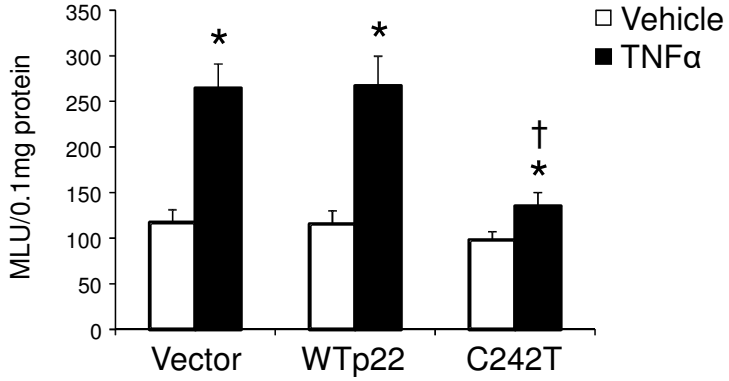


HPMEC membrane fraction was prepared as described in the method. NADPH-dependent $O_{2}^{\cdot -}$ production was measured by lucigenin (5 µmol/L)-chemiluminescence. *$p$<0.05 for indicated values versus vehicle values in the same gene transfection group. †$p$<0.05 for indicated values versus WT TNFα values.

**Supplemental Figure VI.** Effects of p22$^{phox}$ C242T SNP on high glucose (25 mmol/L)-induced $O_2^{\cdot-}$ production

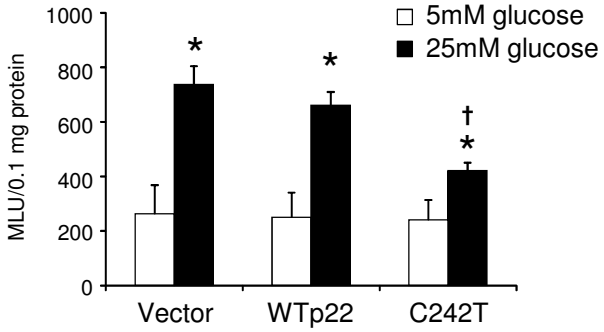


HPMEC were cultured in the presence of normal glucose level (5 mmol/L) or high-glucose level (25 mmol/L) for 24 h. NADPH-dependent $O_2^{\cdot-}$ generation by cell homogenates was measured by lucigenin (5 µmol/L)-chemiluminescence. *$p$<0.05 for indicated values versus 5 mM glucose values in the same gene transfection group. †$p$<0.05 for indicated values versus vector or WT p22$^{phox}$ transfected 25 mmol/L glucose values. n=4 separate gene transfection experiments.

**Supplemental Figure VII.** Colour presentation and quantification of the p22$^{phox}$ fluorescence intensity in HeLa cells presented in Figure 7B

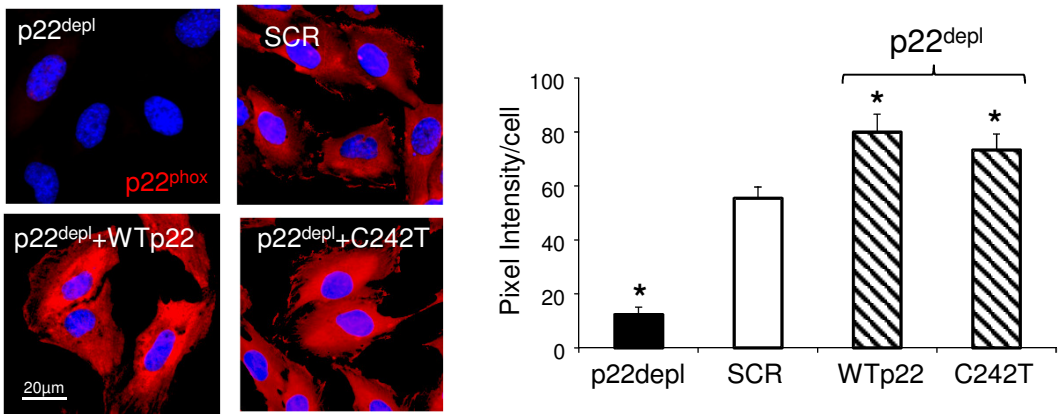


For quantification, results are means ± SD from 30 images of 3 independent experiments. *$p$<0.05 for indicated value versus SCR values.

**Supplemental Figure VIII.** p22$^{phox}$ binding to Nox isoforms in p22$^{phox}$ depleted HeLa cells.

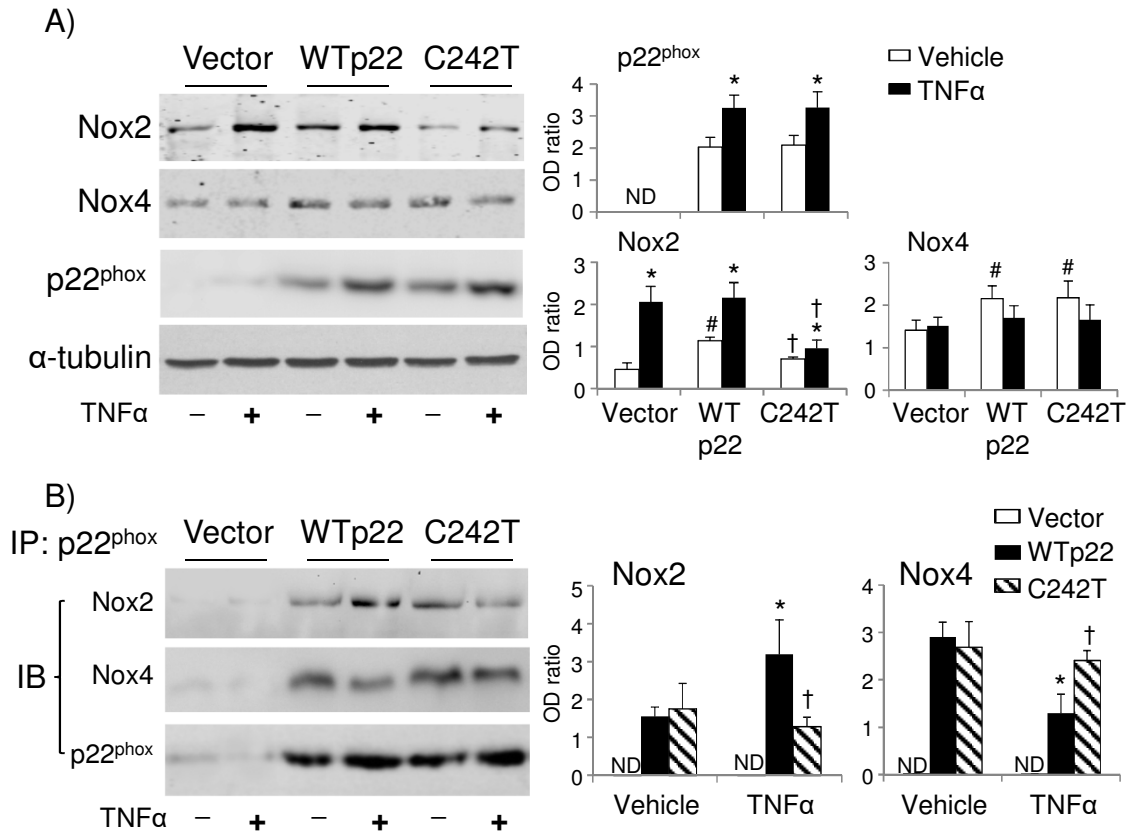


A) Western blots of whole cell homogenates (Input of B). Optical densities (OD) of protein bands were quantified and normalised to α-tubulin detected in the same sample. *P<0.05 for TNFα values versus vehicle values in the same gene transfection group. #P<0.05 for indicated values versus vector vehicle values. †P<0.05 for indicated values versus WTp22 TNFα values. B) p22$^{phox}$ was immunoprecipited (IP) followed by immunoblot (IB). The results were normalized to the levels of total p22$^{phox}$ detected in the same samples. *$p$<0.05 for indicated values versus vehicle values under the same gene transfection. †$p$<0.05 for indicated values versus WTp22 TNFα values. n=4 separate gene transfection experiments.

**Supplemental Figure IX.** TNFα-induced $O_{2}^{\cdot-}$ production by coronary microvascular endothelial cells (CMEC) isolated from WT and Nox2KO mice

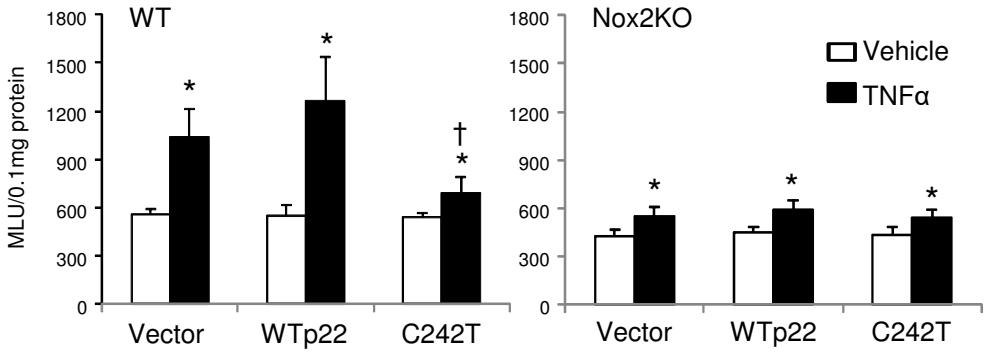


WT and Nox2 knockout (KO) CMEC were transfected with an empty vector or WT $p22^{phox}$ or C242T $p22^{phox}$ plasmids. Cells were then stimulated with TNFα for 30 min. The $O_{2}^{\cdot-}$ production was measured by lucigenin (5 µmol/L)-chemiluminescence. n=3 separate cell isolations (6 mice/per isolation). *$p$<0.05 for indicated values versus vehicle values in the same gene transfection group. †$p$<0.05 for indicated values versus WTp22 TNFα values.

**Supplemental Figure X.** Real-time PCR detection of Nox mRNA expressions in HPMEC.

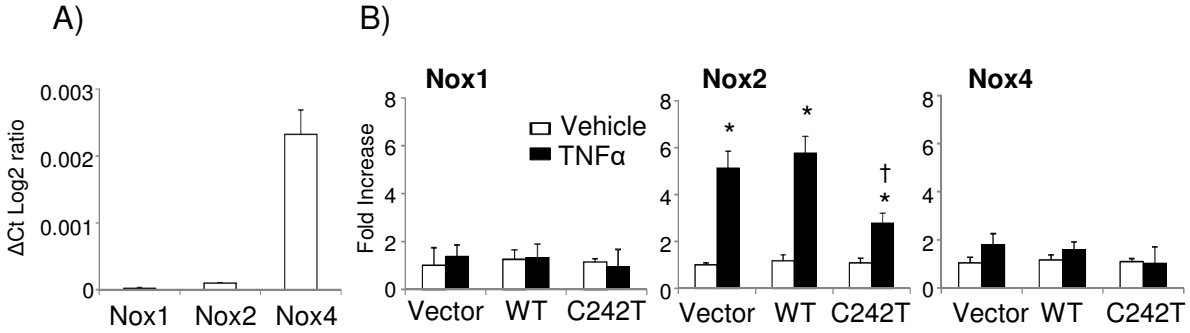


A) Basal Nox1, Nox2 and Nox4 mRNA expression (without TNFα). B) Fold changes of Nox1, Nox2 and Nox4 mRNA expression in response to TNFα (24 h) stimulation. The values of vector transfected control cells for each gene were expressed as 1. *$p$<0.05 for TNFα values versus vehicle values in the same gene transfection group. †$p$<0.05 for indicated values versus WT TNFα values. n=4 independent gene transfection experiments.